The phase diagram for coexisting d-wave superconductivity and charge-density waves: cuprates and beyond

2011 J. Phys.: Condens. Matter 23 385701

(http://iopscience.iop.org/0953-8984/23/38/385701)

IOP PUBLISHING JOURNAL OF PHYSICS: CONDENSED MATTER

J. Phys.: Condens. Matter **23** (2011) 385701 (22pp) doi:10.1088/0953-8984/23/38/385701

The phase diagram for coexisting d-wave superconductivity and charge-density waves: cuprates and beyond

Toshikazu Ekino[1], Alexander M Gabovich[2], Mai Suan Li[3], Marek Pękała[4], Henryk Szymczak[3] and Alexander I Voitenko[2]

[1] Graduate School of Integrated Arts and Sciences, Hiroshima University, Higashi-Hiroshima, 739-8521, Japan
[2] Institute of Physics, National Academy of Sciences of Ukraine, 46, Nauka Avenue, Kyiv 03680, Ukraine
[3] Institute of Physics, Aleja Lotników 32/46, PL-02-668 Warsaw, Poland
[4] Department of Chemistry, University of Warsaw, Aleja Żwirki i Wigury 101, PL-02-089 Warsaw, Poland

E-mail: gabovich@iop.kiev.ua

Received 11 April 2011, in final form 15 July 2011
Published 5 September 2011
Online at stacks.iop.org/JPhysCM/23/385701

Abstract

Phase diagrams of d-wave superconductivity characterized by an order parameter Δ coexisting with charge-density waves (CDWs) characterized by an order parameter Σ were constructed for the two-dimensional Fermi surface (FS) appropriate to, e.g., cuprates. CDWs were considered as an origin of the pseudogap appearing at antinodal FS sections of the $d_{x^2-y^2}$ superconductor. Two types of the Σ-reentrance were found: with the temperature, T, and with the opening of the CDW sector, 2α. The angular plots in the momentum space for the resulting gap profile over the FS ('gap roses') were obtained. The gap patterns are rather involved, giving insight into the difficulties of the interpretation of photoemission spectra. It was shown that the Σ–Δ coexistence region exists even for the complete dielectric gapping due to the distinction between the superconducting and CDW order parameter symmetries. The checkerboard and unidirectional CDW configurations were examined, and both the phase diagrams and the behavior with T and α of the order parameters were found to differ. A more general case with a non-zero mismatch angle β between the superconducting lobes and the CDW sectors was analyzed, the case $\beta = \pi/4$ corresponding to the d_{xy} symmetry of the superconducting order parameter. The phase diagrams were found to be sensitive to β-variations, showing that internal strains and external pressure can drastically affect the behavior of $\Sigma(T)$ and $\Delta(T)$.

(Some figures in this article are in colour only in the electronic version)

1. Introduction

The pseudogap phenomenon is one of the most involved scientific problems in the physics of high-T_c superconductors. At the same time, it remains rather a disappointing issue [1–4], since the lack of consensus concerning the pseudogap nature means the absence of a consistent theory of superconductivity after 25 years of enormous collective efforts (see books and reviews describing various contradicting accounts of the state of art [5–10]). Therefore, it is no wonder that nobody can successfully predict new superconductors and calculate their critical temperatures [11]. Nevertheless, it is conventionally agreed that all versatile theories and concepts concerning pseudogaps can be divided into two categories:

(i) theories based on the concept of precursor (fluctuating) superconductivity [12, 13], which may be transformed below the superconducting critical temperature T_c either into the Bardeen–Cooper–Schrieffer-like (BCS-like) [14, 15] or Bose–Einstein-like [16, 17] superfluid states, and (ii) theories of competing order [12, 18–22]. There are also a few hybrid approaches [23].

We are not going to talk in detail about numerous different theoretical approaches indicated above and discussed earlier in comprehensive reviews [24–26]. Instead, in this section, we shall consider only one scenario, proposed by the authors many years ago [18, 19, 27–30] (see also [9–11, 31–43]), and outline experimentally supported arguments for the validity of our viewpoint. In the framework of this scenario, charge-density waves (CDWs) comprise the competing phenomenon interfering with superconductivity in cuprates, especially in underdoped samples. The theory of coexisting d-wave superconductivity and CDWs [11, 44–46] will be applied in the subsequent sections of the paper to the construction of the phase diagram of cuprates and description of various possible mixed CDW superconducting states.

It is well known that structural anomalies—called periodic lattice distortions (PLDs)—accompanied by electron-density modulations (CDWs) [47] were indeed observed in various high-T_c oxides [1, 9–11, 36–38, 48]. One should distinguish between checkerboard superstructures [49–54], being quite natural for the electron distribution with fourfold rotational symmetry inherent to cuprates with their quasi-two-dimensional CuO_2 planes [25, 55–57], and distorted states with broken rotational symmetry, e.g., unidirectional CDWs [51, 52, 58–61] or more disordered nematic configurations [1, 48, 62, 63]. If thin static or fluctuating charged domains alternate with spin-ordered ones, i.e. a peculiar unidirectional phase separation occurs (more general phase separation scenarios were proposed long ago for versatile objects [64]), the electronic state of a crystal is frequently called a stripe phase [1]. One should also bear in mind the possibility of loop-current electron ordering [1, 48], going back to states predicted for the excitonic insulator [65].

We shall examine both checkerboard and unidirectional CDWs, which can be easily treated on an equal footing with each other [45]. The first situation was found in $Ca_{2-x}Na_xCuO_2Cl_2$ [66, 67], $Bi_2Sr_2CaCu_2O_{8+\delta}$ [50, 68–72], $Bi_2Sr_{2-x}La_xCuO_{6+\delta}$ [73, 74], $Bi_{2-y}Pb_ySr_{2-z}La_zCuO_{6+x}$ [75], whereas the second one was observed in $La_{1.875}Ba_{0.125}CuO_4$ and $La_{1.875}Ba_{0.075}Sr_{0.05}CuO_4$ [76], $La_{1.8-x}Eu_{0.2}Sr_xCuO_4$ [77], $Ca_{1.88}Na_{0.12}CuO_2Cl_2$ and $Bi_2Sr_2Dy_{0.2}Ca_{0.8}Cu_2O_{8+\delta}$ [61], $Bi_{2+x}Sr_{2-x}CuO_{6+\delta}$ [78], $Bi_{2-x}Pb_xSr_2CaCu_2O_{8+y}$ [79], and $Bi_2Sr_2CaCu_2O_{8+\delta}$ [80, 81]. It is crucial that CDWs were shown to exist both below and above T_c. We also emphasize that different kinds of modulations were found for the same material, $Bi_2Sr_2CaCu_2O_{8+\delta}$ [50, 68–72, 80, 81]. A transition from unidirectional to checkerboard CDWs may be stimulated, e.g., by doping, as in the case of $YBa_2Cu_3O_{7-\delta}$, where a Lifshitz topological transition occurs at a hole concentration of 0.08 [82, 83].

It turned out to be very instructive that measurements of transport and photoemission properties in non-superconducting layered nickelates $R_{2-x}Sr_xNiO_4$ (R = Nd, Eu), structurally similar to cuprates, revealed a correlation between the pseudogap emergence and charge ordering [84]. Pseudogaps appeared on the same Fermi surface (FS) sections as in cuprates evidencing the similarity between two classes of materials. Layered dichalcogenides constitute another group of materials with CDWs [47] similar to those in cuprates, as has been recently shown [85–88] (see also [35]). In particular, a true pseudogap—a non-mean-field fluctuation precursor phenomenon [89]—is observed in 2H-$TaSe_2$ above the normal metal–incommensurate CDW transition temperature $T_{N-IC} \approx 122$ K [85]. Such a behavior comprises a strong argument in favor of the CDW nature of pseudogapping in cuprates as well.

The scenario adopted, like a number of others, considers two competing order parameters and two characteristic temperatures, whereas the actual situation, at least in some high-T_c oxides, may be more involved. For instance, precursor phenomena were observed in the infrared spectra of $RBa_2Cu_3O_{7-\delta}$ (R = Y, Gd, Eu) alongside pseudogapping and well-developed superconductivity [90].

There are two more aspects which are important when formulating the approach to the pseudogap enigma in high-T_c oxides. First, there is the intrinsic inhomogeneity of the spatial distribution of CDW order parameter over the samples. This circumstance is not important for the thermodynamic theory presented, although it becomes extremely significant and sometimes crucial, e.g., for the analysis of current–voltage characteristics of tunnel junctions involving high-T_c superconductors (see [11, 42, 91–94]). Another aspect is the symmetry of the superconducting order parameter. The problem is far from being solved [95–97]. Hereafter, we shall restrict ourselves to the $d_{x^2-y^2}$-wave superconductivity [98, 99], in accordance with the majority of experiments [100]. Possible states with intrinsic or extrinsically induced angular (in the momentum space) deviations from $d_{x^2-y^2}$ symmetry, including the d_{xy} state [15, 55, 96, 101–104], will be also considered for generality.

The outline of the paper is as follows. In section 2, the theoretical formulation is presented, whereas section 3 contains analytical and numerical results, as well as relevant discussions. Short conclusions are given in section 4.

2. Theory

Our model for the CDW $d_{x^2-y^2}$-wave superconductivity [44, 45] is a generalization of earlier theories [11, 22, 105, 106] dealing with the interplay between the isotropic s-wave Cooper pairing and CDWs. We shall present below a short formulation of the problem, a more detailed version of which can be found in our paper [45]. In this paper, we restrict ourselves to the 'pure' $d_{x^2-y^2}$ superconductivity bearing in mind that orthorhombic distortions—in particular, for $YBa_2Cu_3O_{7-\delta}$ [107]—allow the appearance of a state with a combined s + d order parameter [15, 102]. The coexistence of such a state with CDWs should be rather complicated, since, as is shown below, the phase diagram of the CDW $d_{x^2-y^2}$-wave superconductor itself is rather

complicated, being substantially different from that for CDW s-wave superconductor [11, 22].

In essence, the CDW d superconductor is a combination of two 'parent' states: the CDW metal and the d-wave BCS superconductor. They interfere with each other, because of the struggle for the same states on the same FS. At temperatures $T < T_{\rm d}$, the FS of the CDW metal is partially gapped (dielectrically gapped) at the sections (in pairs, j_1 and j_2), which are congruent to each other (nested, d) and where the quasiparticle spectrum $\xi(\mathbf{p})$ is degenerate,

$$\xi_{j_1}(\mathbf{p}) = -\xi_{j_2}(\mathbf{p}+\mathbf{Q}_j). \tag{1}$$

Here, $\mathbf{Q}_j$ are vectors connecting the j th couple of FS sections. The remaining FS part is non-dielectrized (nd, non-gapped by electron–hole pairing), and its quasiparticle spectrum $\xi_{\rm nd}(\mathbf{p})$ is non-degenerate. The mean-field electron–hole pairing Hamiltonian responsible for CDWs has the form

$$\mathcal{H}_{\rm CDW} = -\tfrac{1}{2}\sum_{j=(j_1,j_2)}\Sigma_j(T)\sum_{\mathbf{p};\alpha=\uparrow,\downarrow} a^{\dagger}_{j_1\mathbf{p}\alpha}a_{j_2\mathbf{p}+\mathbf{Q}_j\alpha} + \text{c.c.} \tag{2}$$

Here, Planck's constant $\hbar = 1$, $a^{\dagger}_{j\mathbf{p}\alpha}$ ($a_{j\mathbf{p}\alpha}$) is the creation (annihilation) operator of a quasiparticle with the momentum $\mathbf{p}$ in the jth branch of the electron spectrum and with the spin projection $\alpha = \pm\frac{1}{2}$. The quantity $\Sigma_j(T)$ is a T-dependent order parameter of the jth CDW existing below the relevant critical temperature $T_{\rm d}$. We consider it uniform within the corresponding nested FS sections (j_1 and j_2). Summation in (2) is carried out over the dielectrically gapped FS sections only, i.e. over the pairs of sections $j = (j_1, j_2)$ connected by the wavevectors $\mathbf{Q}_j$. In our phenomenological approach, the mechanism of CDW generation [38, 47, 85–88, 101, 108, 109] is not specified, and any information concerning the strength of dielectric pairing is implicitly contained in the relevant constants $\Sigma_{j0} = \Sigma_j(T = 0)$. In practice, it may be impossible to distinguish between electron–phonon and Coulomb (excitonic) contributions to pairing interactions in Cooper or electron–hole channels. Such a situation has been recently analyzed [110] using the intercalated CDW superconductor Cu_xTiSe_2 [111] and pure $TiSe_2$, which becomes a superconductor under pressure [112], as examples.

Note that we use the general form of nesting condition (1), which may be the case for different kinds of quasiparticle spectra, e.g., for two-dimensional ones in the tight-binding approximation. However, any such specification would not change our results qualitatively.

As for the parent $d_{x^2-y^2}$ superconductor, we treat it as a weak-coupling one [98, 99] and suggest a strong mixing of states from different FS sections leading to a unique superconducting order parameter $\Delta(T)$ [27, 105]:

$$\mathcal{H}_{\rm d-BCS} = -\sum_{\mathbf{p}}\Delta(T)f(\mathbf{p}) \times\left[\sum_{j=(j_1,j_2)} a^{\dagger}_{j_1\mathbf{p}\uparrow}a^{\dagger}_{j_2-\mathbf{p}\downarrow} + a^{\dagger}_{\rm nd,\mathbf{p}\uparrow}a^{\dagger}_{\rm nd,-\mathbf{p}\downarrow}\right] + \text{c.c.} \tag{3}$$

The angular factor $f(\mathbf{p})$ describes the order parameter symmetry. The summation in (3) is executed over the whole FS. The Cooper pairing strength is determined by the parameter $\Delta_0 = \Delta(T = 0)$.

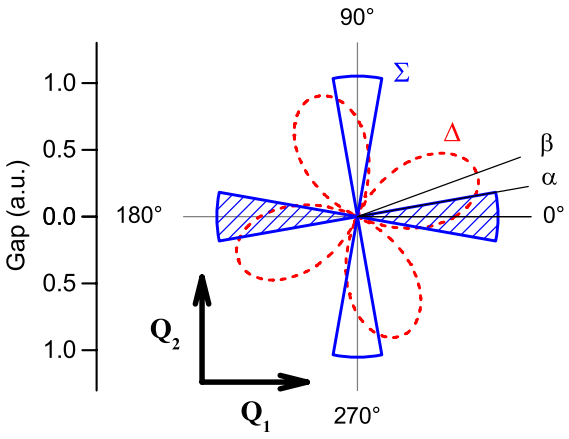

Figure 1. Superconducting (Δ, dashed curve) and dielectric (Σ, solid curve) order parameter profiles on the Fermi surface (FS) in two-dimensional momentum space for the parent phases of the d-wave superconductor and the partially gapped metal with charge-density waves (CDWs), respectively, i.e. when the competitive pairing channel is switched off. $\mathbf{Q}_1$ and $\mathbf{Q}_2$ are the CDW vectors, 2α is the opening of each CDW-gapped sector, β is the mismatch angle between the superconducting lobes and CDW sectors. The checkerboard CDW configuration is described by both wavevectors $\mathbf{Q}_1$ and $\mathbf{Q}_2$, and it includes all four CDW sectors; the unidirectional one is described by one wavevector $\mathbf{Q}_1$, and it includes two hatched CDW sectors.

The kinetic energy term in the Hamiltonian is conventional, making allowance for all FS sections:

$$\mathcal{H}_0 = \sum_{i=j_1,j_2,\rm nd}\sum_{\mathbf{p};\alpha=\uparrow,\downarrow}\xi_i(\mathbf{p})a^{\dagger}_{i\mathbf{p}\alpha}a_{i\mathbf{p}\alpha}. \tag{4}$$

Now, let us specify the model further, making it closer to the experiment. First of all, it allows us to confine the consideration to the 2D case in the momentum space. Experimentally, two CDW configurations are observed in high-$T_{\rm c}$ oxides. In the unidirectional one, there exists a single CDW described by a single wavevector $\mathbf{Q}_1$. In the checkerboard configuration, there are two CDWs described by two mutually orthogonal vectors $\mathbf{Q}_1$ and $\mathbf{Q}_2$ with almost equal magnitudes. We shall describe both of those geometries as is depicted in figure 1. We adopt the convention that the CDW vector $\mathbf{Q}_1$ which connects two dielectrically gapped FS sections in the unidirectional geometry (this case is marked by hatched lobes) is parallel to the p_x-axis. Each section has the angular width 2α, independent of the temperature T. Two more gapped sections are added about the p_y-axis in the case of checkerboard geometry, characterized by two mutually perpendicular CDW vectors $\mathbf{Q}_1$ and $\mathbf{Q}_2$ (four lobes with a solid boundary in figure 1). We adopt the convention that, except as regards the orientation, the nested FS sections are identical, being measured by the same angle 2α and dielectrically gapped to the same uniform amplitude $\Sigma(T)$. In this case, instead of describing every pair of dielectrically gapped sections separately, we may introduce a unique parameter of FS dielectric gapping degree $\mu(0 \le \mu \le 1)$, the fraction of dielectrically gapped states on the FS [11, 22,

106]. The sections are located symmetrically with respect to the corresponding axes so that the bisectrices of dielectrically gapped sectors—in this way, we fix the positions of the nested FS sections—coincide with the axes.

As regards the distribution of superconducting gap Δ over the FS of the parent d superconductor in the 2D geometry, the angular factor in formula (3) has the form $f(\mathbf{p}) = \cos 2\theta$, where the angle θ is reckoned from a certain direction in the 2D momentum space denoted by the angle β. In the $d_{x^2-y^2}$ state, the Δ-lobes are directed along the p_x- and p_y-axes [104, 113], so that the mismatch angle β between the 'superconducting' and 'dielectric' lobes in the parent metals is zero ($\beta = 0$). Moreover, according to the experiment, sectors with non-zero pseudogap (in our interpretation, the CDW gap, Σ) are competing with superconductivity exactly in those—the most vulnerable to the obstacle—antinodal regions [40, 114–116]. (Those FS sections in high-T_c cuprates are sometimes called 'hot spots' [3, 9, 10].) Nevertheless, we would like to extend the range of system parameters and consider also the case $\beta \neq 0$, a more general model than that describing actual hole-doped cuprates. Thus, we assume that the CDW directions remain fixed with respect to the background crystal lattice. At the same time, the superconducting lobes can be rotated by the angle β round the 2D Brillouin zone axis. Note that if $\beta = \pi/4$, the superconducting state becomes the hypothetical d_{xy} one [15, 55, 96, 102–104]. In all the intermediate states with $\beta \neq 0$ or $\pi/4$, the conventional angular symmetry is broken, but such states may exist in real distorted crystals, as well as under an applied non-hydrostatic external pressure. This picture is appropriate to the checkerboard situation, while for the unidirectional configuration, we actually deal with stripe patterns, although without any antiferromagnetic domains [117]. It turned out to be instructive to compare the two cases.

It is evident that the problem is invariant with respect to the system rotation in the momentum space by the angle $\Omega = \pi$ in the unidirectional case with the number of CDW sectors $N = 2$, and $\Omega = \pi/2$ in the checkerboard one with $N = 4$. It is easy to see that the parameters μ, α, N, and Ω are coupled by the relations

$$\mu\Omega = 2\alpha, \tag{5}$$

$$N\Omega = 2\pi. \tag{6}$$

These formulas demonstrate that the parameter α can vary from 0 ($\mu = 0$, the absence of FS dielectric gapping) to $\pi/2$ in the unidirectional CDW configuration (the case of full FS gapping, $\mu = 1$, and $N = 2$) and to $\pi/4$ in the checkerboard one ($\mu = 1, N = 4$). As we shall see below, the gapping degree parameter α is more informative than μ.

The total Hamiltonian of the electron subsystem is a sum of three terms (2)–(4). The quantities Σ_0, Δ_0, μ, Ω, and the mismatch angle β between the bisectrices of CDW sectors and superconducting lobes constitute the full set of the problem input parameters. They are phenomenological constants that can be, in principle, reconstructed from the experimental data. For instance, such a possibility exists for the ratio μ between the dielectrized portion of the FS and the total length of the FS in the 2D Brillouin zone. The many-body correlation effects different from those described by the pairing terms (3) and (2) in the Hamiltonian are incorporated into μ, since the very form of the FS calculated in microscopic and semi-microscopic models depends on the electron–electron interaction [118, 119].

In a standard way [22, 38, 45, 120], from Dyson–Gor'kov equations, we obtain the Green's functions describing the electron component of our CDW superconductor and insert them into self-consistency equations for the self-energy parts $\Sigma(T)$ and $\Delta(T)$. The resulting solutions are implicitly given by the following system of coupled integral equations:

$$\int_{-\alpha}^{\alpha} I_M\left(\sqrt{\Sigma^2 + \Delta^2\cos^2 2(\beta+\theta)}, T, \Sigma_0\right) d\theta = 0, \tag{7}$$

$$\int_{\beta-\alpha}^{\beta+\alpha} I_M\left(\sqrt{\Sigma^2 + \Delta^2\cos^2 2\theta}, T, \Delta_0\cos 2\theta\right)\cos^2 2\theta\, d\theta + \int_{\beta+\alpha}^{\Omega+\beta-\alpha} I_M(\Delta\cos 2\theta, T, \Delta_0\cos 2\theta)\cos^2 2\theta\, d\theta = 0, \tag{8}$$

where the Boltzmann constant $k_B = 1$, and the quantity

$$I_M(\Delta, T, \Delta_0) = \int_0^{\infty}\left(\frac{1}{\sqrt{\xi^2+\Delta^2}}\tanh\frac{\sqrt{\xi^2+\Delta^2}}{2T} - \frac{1}{\sqrt{\xi^2+\Delta_0^2}}\right) d\xi \tag{9}$$

is the so-called Mühlschlegel integral [121] of the BCS theory. Note that it is more reasonable to reckon the integral variable θ in integral (8) from the superconducting lobe maximum direction, i.e. from the ray corresponding to the angle β, since the formula looks less cumbersome in this case.

It is convenient to introduce the dimensionless temperature $t = k_B T/\Delta_0$ as well as order parameters $\sigma(t) = \Sigma(T)/\Delta_0$ ($\sigma_0 = \Sigma_0/\Delta_0$) and $\delta(t) = \Delta(T)/\Delta_0$ ($\delta_0 \equiv 1$). Then, (7) and (8), taking relations (5) and (6) into account, read

$$\int_{-\alpha}^{\alpha} I_M\left(\sqrt{\sigma^2 + \delta^2\cos^2 2(\beta+\theta)}, t, \sigma_0\right) d\theta = 0, \tag{10}$$

$$\frac{8}{N}\int_0^{\pi/4} I_M(\delta\cos 2\theta, t, \cos 2\theta)\cos^2 2\, d\theta + \int_{\beta-\alpha}^{\beta+\alpha}\left[I_M\left(\sqrt{\sigma^2+\delta^2\cos^2 2\theta}, t, \cos 2\theta\right) - I_M(\delta\cos 2\theta, t, \cos 2\theta)\right]\cos^2 2\theta\, d\theta = 0. \tag{11}$$

Equations (10) and (11) differ from those analyzed in [44] by the introduction of the mismatch angle β and a possibility of treating unidirectional CDWs, in addition to the checkerboard ones, using the same system of equations.

If superconductivity is absent ($\delta = 0$), (10) is reduced to the gap equation [122] for the parent CDW metal

$$I_M(\sigma, t, \sigma_0) = 0, \tag{12}$$

while (8), when the dielectrization is absent ($\sigma = 0$ or $\alpha = 0$), becomes the equation for a d-wave BCS weak-coupling superconductor

$$\int_0^{\pi/4} I_{\mathrm{M}}(\delta \cos 2\theta, t, \cos 2\theta)\cos^2 2\theta \, \mathrm{d}\theta = 0. \qquad (13)$$

Therefore, it is convenient to introduce the following mnemonic terms: 'σ-equation' for (10) and 'δ-equation' for (11). The well-known solutions of (12) and (13) are given by tabulated functions $\sigma = M\ddot{u}_{\mathrm{s}}(\sigma_0, t)$ and $\delta = M\ddot{u}_{\mathrm{d}}(1, t)$, respectively [98, 99, 120, 123].

Note that, in the specific case of interplay between s-wave CDWs and d-wave superconductivity, the order parameters do not change their phases under the influence of their counterparts. This independence may be violated in superconductors with spin-density waves, where the order parameter spin structures are different, with the result that various situations become possible [124–126].

To make subsequent expressions more compact, let us introduce the following notation: $R_{\mathrm{s}} = \Sigma_0/T_{\mathrm{d}0} = \frac{\pi}{\gamma} \approx 1.764$, where $\gamma \approx 1.781$ is the Euler constant, is the ratio between the zero-T gap value and the critical temperature for the BCS s-wave superconductor (according to (12), it is also appropriate to the relevant parameters Σ_0 and $T_{\mathrm{d}0}$, respectively, of the parent CDW metal); $R_{\mathrm{d}} = \Delta_0/T_{\mathrm{c}0} = \frac{2}{\sqrt{\mathrm{e}}}\frac{\pi}{\gamma} \approx 2.140$, where e is the base of natural logarithms, is the analogous ratio for the BCS d-wave superconductor; and the ratio between those two quantities $\bar{\sigma}_0 = R_{\mathrm{s}}/R_{\mathrm{d}} = \frac{\sqrt{\mathrm{e}}}{2} \approx 0.824$. The usage of functions $M\ddot{u}_{\mathrm{s}}(\sigma_0, t)$ and $M\ddot{u}_{\mathrm{d}}(\sigma_0, t)$ means that they vanish above the corresponding critical temperatures: $M\ddot{u}_{\mathrm{s}}(1, t \geq R_{\mathrm{s}}^{-1} \approx 0.567) = 0$ and $M\ddot{u}_{\mathrm{d}}(1, t \geq R_{\mathrm{d}} \approx 0.467) = 0$.

Our self-consistent system of equations for order parameters corresponds to the free energy minimum, like what was shown for pure BCS superconductors [99, 103] and CDW s-wave ones [22]. Nevertheless, it would be instructive to show it directly, and this is especially interesting in view of the application to the specific heat. This will be done in a subsequent publication.

3. Results of calculations

Earlier [44], we found that d-wave superconductors partially gapped by CDWs can exhibit a reentrance behavior of the dielectric order parameter $\Sigma(T)$ in the temperature domain for some particular values of the dimensionless parameters $\sigma_0 = \Sigma_0/\Delta_0$ and α (or, what is the same, $\mu = 2\alpha/\Omega$). In this paper, we are going to extend the scope of the analysis and construct the overall phase diagram of the CDW d superconductor on the σ_0–α plane. The mismatch angle β between the bisectrix of one of the CDW sectors, being closest to $\theta = 0$, and the $\theta = 0$ position of a certain superconducting order parameter maximum (the lobe maximum) serves as an additional parameter, describing a possible symmetry breaking, if $\beta \neq 0$ or $\pi/4$ (checkerboard case) or $\beta \neq 0$ or $\pi/2$ (unidirectional case). For cuprates, experimental data demonstrate that $\beta = 0$ [40, 114–116]. A pattern with a broken symmetry might be due to internal residual strains in the sample, a non-homogeneous distribution of the dopant atoms, an influence of out-of-plane structural elements (such as chains in $YBa_2Cu_3O_{7-\delta}$ [48, 63]) or the deliberate switching on of external factors, e.g., uniaxial pressure.

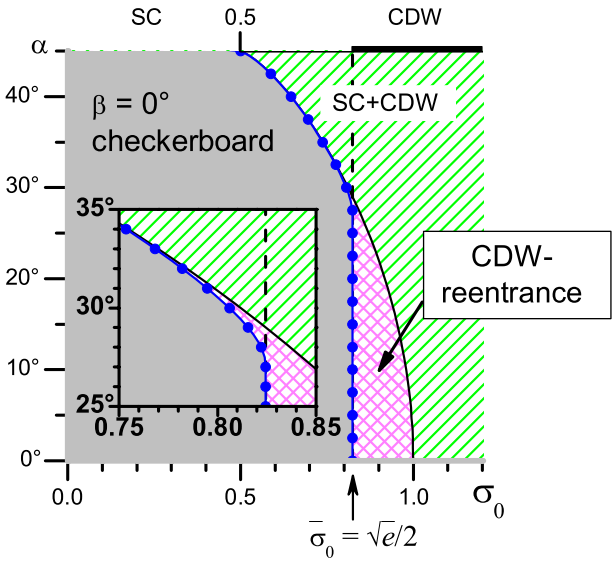

Figure 2. Phase diagram of a CDW $d_{x^2-y^2}$ superconductor ($\beta = 0°$) in the checkerboard configuration on the α–σ_0 plane. $\sigma_0 = \Sigma_0/\Delta_0$ is the relative strength of the CDW (electron–hole) pairing, Σ_0 the order parameter magnitude for the parent CDW phase at zero temperature ($T = 0$), Δ_0 the superconducting (SC) order parameter magnitude for the parent d-wave superconducting phase at $T = 0$. The gray region corresponds to the pure SC phase, where CDWs are absent at any T, the hatched one to the combined SC + CDW phase, and the CDW-reentrance (cross-hatched) one to the phase, where the superconductivity and CDWs coexist in a certain T-interval $0\ \mathrm{K} < T_{\mathrm{r}} < T < \min(T_{\mathrm{d}}, T_{\mathrm{c}})$. Here, T_{r} and T_{d} are the lower and upper CDW critical temperatures, respectively, and T_{c} is the SC critical temperature. Gray sections of the phase diagram correspond to the pure SC phase. The bold black line along the upper phase diagram boundary denotes the range of pure CDW phase existence. The scaled-up fragment of the phase diagram is shown in the inset.

It is worth mentioning that the choice of dimensionless parameter $\sigma_0 = \Sigma_0/\Delta_0$—i.e. the normalization by $\Delta_0 \neq 0$—implies the obligatory presence of Cooper pairing in the model concerned, irrespective of whether the mechanism of dielectric pairing is engaged or not. Thus, all possible (σ_0, α)-combinations at a fixed β fill the whole semi-infinite ($\sigma_0 \geq 0$) strip on the σ_0–α plane between the ordinates $\alpha = 0$ and $\pi/4$, in the case of the checkerboard CDW configuration, and between $\alpha = 0$ and $\pi/2$, in the case of the unidirectional one. Since the former case is observed much more frequently, let us analyze it first.

3.1. The checkerboard CDW configuration ($N = 4$, $\Omega = \pi/2$)

3.1.1. Zero-value mismatch angle between CDW sectors and superconducting lobes: $\beta = 0$. This is the case observed experimentally in cuprates, so it deserves to be a starting point.

Two loci in the α–σ_0 phase diagram are trivial, both corresponding to the total absence of CDWs. These are (see figure 2) the case $\alpha = 0$ (the positive abscissa semi-axis)

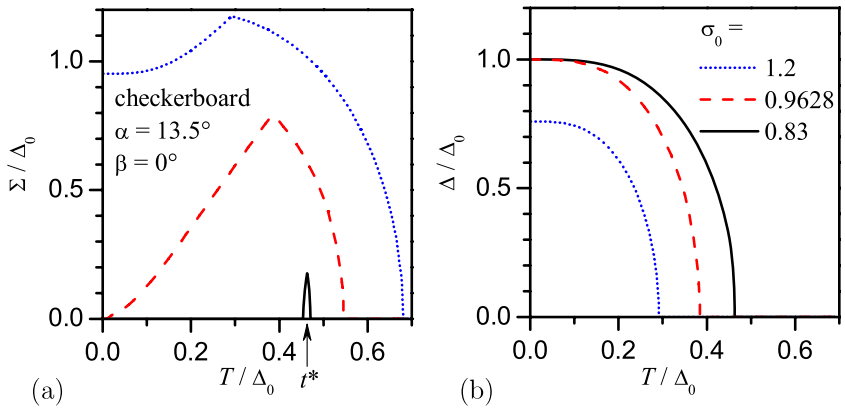

Figure 3. Normalized temperature dependences of (a) the CDW, Σ, and (b) the superconducting, Δ, order parameters for various σ_0 in the checkerboard configuration. t^* is the normalized reentrance-collapse temperature (see explanations in the text).

and the case $\sigma_0 = 0$ (the whole sector $0 \leq \alpha \leq \pi/4$ in the checkerboard configuration) along the ordinate axis (α-axis) representing the parent $d_{x^2-y^2}$-wave BCS superconductor. It is also clear that, except for the limiting case of complete FS dielectrization, the configuration of partial gapping implies the existence of an nd-section (an 'open back door') on the FS, through which superconductivity could always 'penetrate'. Therefore, the partially gapped CDW d superconductor preserves superconductivity at almost every point of the phase diagram presented. Nevertheless, two questions are to be answered, as follows. (i) To what extent can CDWs suppress superconductivity? (ii) Can superconductivity completely destroy CDWs?

The third border of the phase diagram ($\alpha = \pi/4$), which corresponds to the case of complete FS dielectrization, will be considered in section 3.1.2 in more detail.

Let us study the phase diagram by scanning it along characteristic paths. Namely, we intend to consider the evolution of $\Sigma(T)$- and $\Delta(T)$-dependences with varying σ_0 for a few fixed α-values. Let $\alpha = 13.5°$, which corresponds to $\mu = 0.3$ (figure 3). We start from the phase point located in the region of large σ_0, which is designated as SC + CDW (see figure 2). Here, both order parameters, Σ and Δ, exist within the corresponding temperature intervals—$0 \leq T < T_d$ and $0 \leq T < T_c$, respectively. For the chosen parameter value $\sigma_0 = 1.2$, the superconducting critical temperature is lower than its CDW counterpart: $T_c < T_d = T_{d0}$, and both order parameters extend to $T = 0$. The concave section in the $\Sigma(T)$-dependence is a result of the detrimental action of the Cooper pairing on dielectric instability [11, 22, 36–38, 105, 127–131]. It should be emphasized that such a nonmonotonic behavior of $\Sigma(T)$ does not violate the monotonic t-dependences of the gaps—$\Delta(T)\cos 2\theta$ on the non-nested and $\sqrt{\Sigma^2(T) + \Delta^2(T)\cos^2 2\theta}$ on the nested FS sections [45].

A decrease of the parameter σ_0 corresponds to a reduction of the CDW pairing strength. First, it results in a stronger detrimental action of the superconducting gap on Σ in the interval of their coexistence, so Σ decreases (figure 3(a)). Second, the reciprocal detrimental action of CDWs on superconductivity weakens, which manifests itself in a widening of the T-interval of superconductivity (T_c grows; figure 3(b)). When the moving phase point crosses the border between the SC + CDW region and the region denoted as CDW-reentrance (it occurs at $\sigma_0 \approx 0.9628$ if $\alpha = 13.5°$), the lowest-T starting point of the dependence $\Sigma(T)$ falls into the coordinate origin ($\Sigma(T = 0) = 0$). From what follows, it is convenient to call this event the 'reentrance-start' and the locus of corresponding points in the phase diagram the 'reentrance-start boundary'. The corresponding σ_0-value will be denoted as σ_0^{**}. The relationship between the problem parameters for this phenomenon to happen can be easily derived from (10) by putting there $t = 0$, $\sigma = 0$, and $\delta = 1$ to obtain

$$2\alpha \ln \sigma_0^{**} = \int_{\beta-\alpha}^{\beta+\alpha} \ln|\cos 2\theta|\, \mathrm{d}\theta. \tag{14}$$

Note that (14) was written for the general case $\beta \neq 0$. Starting from this phase point, toward lower σ_0 s ($\sigma_0 < \sigma_0^{**}$), we fall into a region where CDWs are restricted to finite T-intervals with non-zero starting points T_r: $0 < T_r < T < T_d$. That is, dielectric gapping does not reveal itself in a certain temperature range above $T = 0$, being effectively hidden ($\Sigma_0 \neq 0$) [44]. We introduce the term 'reentrance temperature' for T_r. Mathematically, this means that (10) with the substitutions $\sigma = 0$ and $\delta = M\ddot{u}_d(t)$ has two t-roots, $t_r = T_r/\Delta_0$ and $t_d = T_d/\Delta_0$.

A further decrease of σ_0 at fixed $\alpha = 13.5°$ brings about a shrinkage of the $\Sigma(T)$-dome and, ultimately, to its collapse. In effect, this collapse results from the convergence of temperatures T_r and T_d to the temperature T^* (the dimensionless parameter $t^* = T^*/\Delta_0$). It is natural to call this event a 'reentrance-collapse' and the locus of the corresponding points in the phase diagram the 'reentrance-collapse boundary'. It should be emphasized that, in the case now examined, $\beta = 0°$ and $\alpha = 13.5°$, the normalized temperatures t_r and t_d converge to the value $t^* = t_{c0} = T_{c0}/\Delta_0$, and the collapse of the $\Sigma(T)$-dome occurs at $\sigma_0^* = \bar{\sigma}_0$ (see appendix A). To the left from the CDW-reentrance region, when continuing the motion along a horizontal straight line with $\alpha = 13.5°$ until $\sigma_0 = 0$, it is possible to find only such states where CDWs are completely

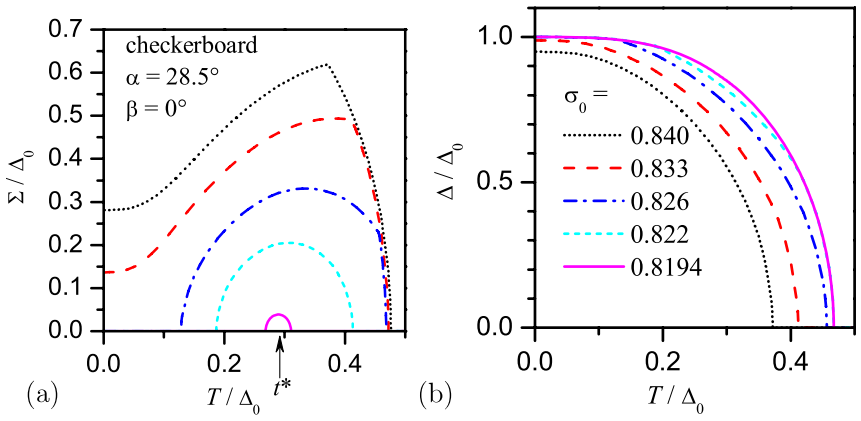

Figure 4. The same as figure 3, but for $\alpha = 28.5°$.

suppressed, i.e. pure d-wave BCS ones [98, 99]. Figure 3(b) demonstrates that the character of the $\Delta(T)$-dependence does not change qualitatively within the whole interval of σ_0-change.

Such a behavior—for both $\sigma(t)$- and $\delta(t)$-dependences—with varying σ_0 remains qualitatively the same within a certain α-range starting from $\alpha = 0$. In particular, there is always a t-region $0 \leq t < t_c$ with $\delta(t) \neq 0$. On the other hand, CDW order can emerge only if $\sigma_0 > \bar{\sigma}_0$ ($t_{d0} > t_{c0}$). At large σ_0 s, the $\sigma(T)$-dependence is nonmonotonic, growing with t in the range $0 \leq t < t_c$ and decreasing down to zero at $t_c < t \leq t_d$, with a cusp occurring at t_c. At a definite σ_0^{**} determined by (14) (the reentrance-start point), the $\sigma(t)$-behavior acquires a reentrance character (the T-driven reentrance or, according to our classification, reentrance of kind I), which disappears at $\sigma_0 \to \bar{\sigma}_0$ (the reentrance-collapse point) from above.

At the same time, the σ_0-interval where the reentrance phenomenon can be observed becomes narrower, as the parameter α increases (a detailed analysis of this process is described in appendix A). The narrowing of this interval is governed by the leftward shift of the reentrance-start boundary σ_0^{**} of the CDW-reentrance region, which is determined by (14), whereas the reentrance-collapse boundary remains fixed at $\sigma_0^* = \bar{\sigma}_0$. The collapse temperature t^*(see figure 3) also stands still: $t^* = t_{c0}$.

However, after α has reached a certain value (in the case $\beta = 0°$, it is $\alpha_{lim} \approx 27.1°$), the behavior of the system changes. It is associated with the fact that the reentrance-collapse boundary starts to deviate toward smaller σ_0 (see figure 2).

Figure 4 illustrates the interplay between order parameters in this case by showing the evolution of $\Sigma(T)$ and $\Delta(T)$ with varying σ_0 at the fixed $\alpha = 28.5° > \alpha_{lim}$. One can see that the $\Delta(T)$-dependences remain qualitatively the same as above. The $\Sigma(T)$-curves, at first glance, also seem to change as in figure 3. Indeed, as σ_0 decreases, the representing phase point first enters the reentrance regime and afterward approaches the $\Sigma(T)$-collapse. However the curves $\Sigma(T)$ corresponding to $\sigma_0 > \bar{\sigma}_0$ possess a cusp at T_c, whereas the curves with $\sigma_0 < \bar{\sigma}_0$ are smooth, because T_c lies beyond the reentrance T-interval: $T_r < T_d < T_c = T_{c0}$. Hence, we obtain that dielectric gapping can emerge and disappear against the superconducting background (see the curves for $\sigma_0 = 0.822$ and $\sigma_0 = 0.8194$ in figure 4). The $\Sigma(T)$-collapse temperature t^* becomes lower in comparison with the earlier case. Figure 2 demonstrates that the reentrance σ_0-interval is very narrow in this case.

It is even narrower at larger α, but, as the analysis in appendix A testifies, remain finite. To illustrate this statement, let us make one more scan across the phase diagram at a larger $\alpha = 35°$. The analysis presented in appendix B shows that T_c varies very rapidly, when crossing the separatrix σ_0^* at large α. Therefore, we selected σ_0-values that are rather close to the reentrance-collapse point (see figure 5(a)). The reentrance σ_0-range is very narrow here (see figure 2): in between $\sigma_0^* \approx 0.7382$ and $\sigma_0^{**} \approx 0.7387$. Nevertheless, the reentrance phenomenon does exist! It is remarkable that the initially d-wave BCS-like $\Delta(T)$-dependence becomes totally distorted in the boundary region of the phase diagram under the CDW influence. Namely, $\Delta(T)$ is almost arrested in a wide temperature range (see figure 5(b)).

The collapse temperature is lower than in the previous case. If we plot the dependence of t^* versus α, we obtain the curve labeled as $\beta = 0°$ in figure 6. One can see that t^* remains constant (this situation corresponds to the fixed $\sigma_0^* = \bar{\sigma}_0$) only up to a definite α (in the most important case $\beta = 0°$, corresponding to the cuprate order parameter geometry, the limiting value is $\alpha_{lim} \approx 27.1°$). For $\alpha < \alpha_{lim}$ the superconducting critical temperature T_c lies in between the temperatures T_r and T_d, so the relationship among the characteristic temperatures is as follows: $0 < T_r < T_c < T_d = T_{d0}$. For α exceeding α_{lim}, T^* starts to decrease drastically with α, which corresponds to the deviation of σ_0^* from $\bar{\sigma}_0$ toward lower values (see the inset in figure 2). This means that CDWs disappear at certain $\sigma_0^*(\alpha) < \bar{\sigma}_0$.

The phase diagram obtained here and displayed in figure 2 also enabled us to explain the mechanism of the $\Sigma(T)$-reentrance governed by the FS dielectric gapping parameter μ. In the previous paper [44], this phenomenon was revealed while moving along the line $\sigma_0 = 0.9$ on the phase diagram. A more detailed analysis on the basis of figure 2 shows that moving along this line from large $\mu \approx 1$ ($\alpha \approx \pi/4$) we meet the same sequence of phases (SC + CDW →

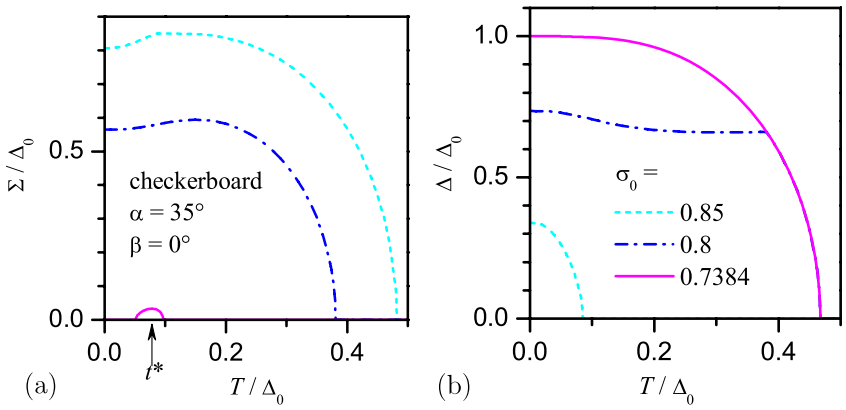

Figure 5. The same as figure 3, but for $\alpha = 35°$.

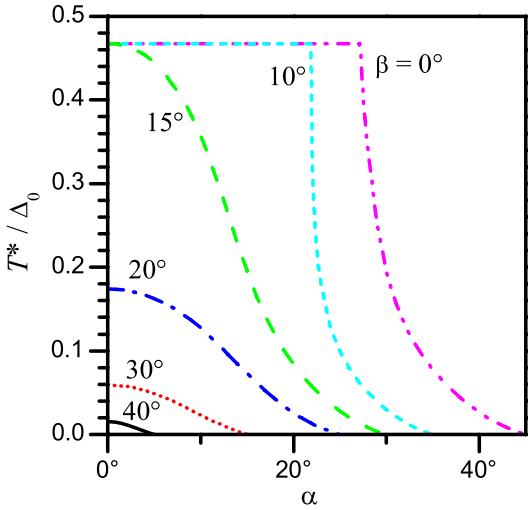

Figure 6. The α-dependences of the normalized reentrance-collapse temperature $t^* = T^*/\Delta_0$ for various mismatch angles β.

CDW-reentrance) as if moving along the path $\alpha = \text{const}$ from larger to smaller σ_0 values.

In other words, the calculations demonstrate that an appearance and subsequent gradual destruction of the $\Sigma(T)$ dome, existing for σ_0 both above and below the value $\bar{\sigma}_0$, may be carried out by decreasing α. In the CDW-reentrance region section to the right from $\sigma_0 = \bar{\sigma}_0$, the pure SC phase is reached only at $\alpha = 0$. On the other hand, the same phase diagram (figure 2) reveals another scenario of the $\Sigma(T)$-reentrance with the appropriate α-interval not extending to zero. Namely, with decreasing α, along, say, $\sigma_0 = 0.8$, the representing point is first located in the SC + CDW region; then, having crossed the start-reentrance separatrix, it enters the CDW-reentrance phase, and, finally, having crossed the other, collapse-reentrance boundary, finds its way into the SC region.

3.1.2. Limiting cases; complete FS dielectrization. The next task is to scrutinize the case of complete FS dielectrization ($\mu = 1$, i.e. $\alpha = \pi/4$ for the checkerboard CDW pattern). The picture turns out to be degenerate with respect to the parameter β, the latter becoming irrelevant. Hence, σ_0 remains the only problem parameter.

For completely gapped CDW s superconductors (when both isotropic order parameters in the parent superconductor and CDW 'metal' are assumed to occupy the whole FS), only one order parameter survives the competition if a possible difference between cutoffs in the Cooper and electron–hole channels is not taken into account [130]. Namely, the parameter with a larger zero-temperature parent amplitude (Σ_0 or Δ_0) or, equivalently, with a larger critical temperature (T_{d0} or T_{c0}, respectively) occupies the whole FS [22]. Thus, if both the superconducting and CDW order parameters are s ones, their coexistence becomes hindered, if not impossible [22, 128–131]

We emphasize that the coexistence of the two order parameters in the case of completely gapped CDW d superconductors is a consequence of their different symmetries. The essence of the problem is that Δ has node points on the FS, through which Σ can 'penetrate'. In this situation, it was found analytically [45] that d superconductivity and CDWs can coexist, although only within the following interval of CDW pairing strength:

$$\tfrac{1}{2} < \sigma_0 < \bar{\sigma}_0. \qquad (15)$$

To the left of this interval ($T_{d0} \leq 0.606 T_{c0}$), our system is a pure BCS d superconductor, whereas to the right ($T_{d0} > T_{c0}$) it becomes a completely gapped CDW insulator (CDWs give no chance for superconductivity to develop). It seems instructive to analyze properties of the completely gapped phase within interval (15) in more detail.

The dependences $\Sigma(T)$ and $\Delta(T)$ for completely gapped CDW d-wave superconductors are depicted in figure 7. Notice an unexpected reverse analogy to the previous results for the coexistence of isotropic pairings. Namely, T-dependences of CDW (superconducting) order parameters are rather similar to those for their superconducting (CDW) counterparts, respectively, inherent to partially gapped CDW s superconductors [22]. In our previous paper [45], we introduced the term 'gap rose' for corresponding angle gap diagrams. The gap roses determine, in particular, which gaps are observed in angle-resolved photoemission (ARPES) spectra. The T-evolution of gap roses for certain σ_0 s is

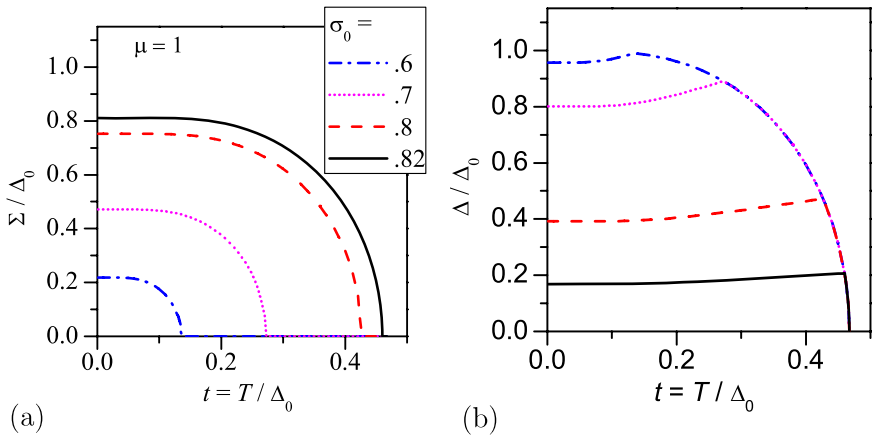

Figure 7. The same as figure 3, but for the complete FS dielectric gapping.

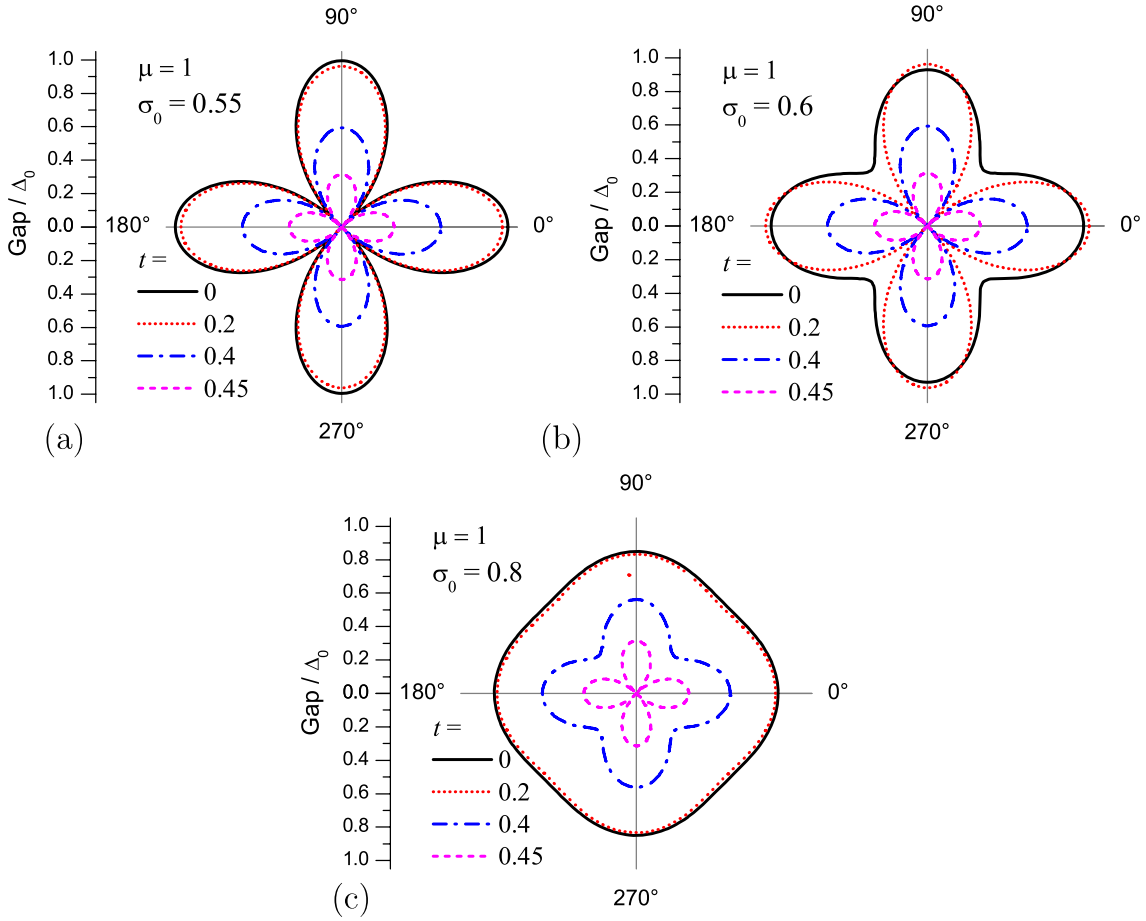

Figure 8. The angle diagrams of the resulting normalized energy gaps on the FS (gap roses) for complete dielectric gapping, various σ_0 (panels (a)–(c)) and normalized temperatures $t = T/\Delta_0$.

displayed in figure 8. Figures 7 and 8 illustrate how the parameter σ_0 governs the process of transformation between a BCS superconductor with d-wave Cooper pairing and a CDW metal with s-wave electron–hole pairing. When σ_0 goes close to the limit $\frac{1}{2}$ (figure 8(a)), the gap configuration has a well pronounced lobe structure, whereas when $\sigma_0 \to \bar{\sigma}_0$ (figure 8(c)) it tends to the isotropic pattern (complete FS dielectrization). Besides, figure 8(b) demonstrates that the combined gap (at $\mu = 1$, the sphere of existence for both order parameters extends over the whole FS) can also reveal a nonmonotonic dependence on T (see the gap roses at $t = 0$ and 0.2 in the vicinity of their maxima).

As was indicated in section 2, each pairing is characterized by the ratio between the zero-temperature order

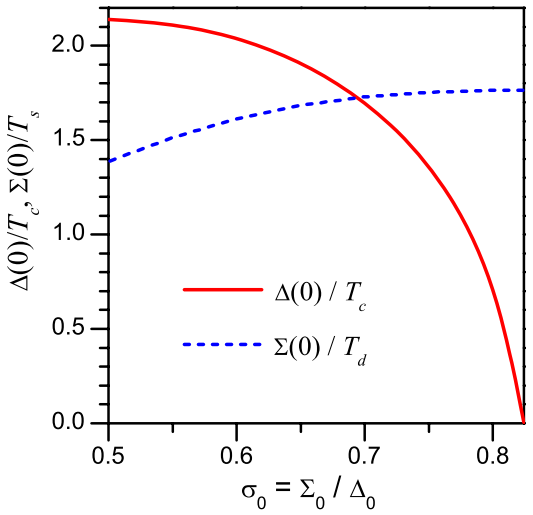

Figure 9. σ_0-dependences of the ratios between the order parameters at $T = 0$ and the relevant critical temperatures for complete CDW gapping.

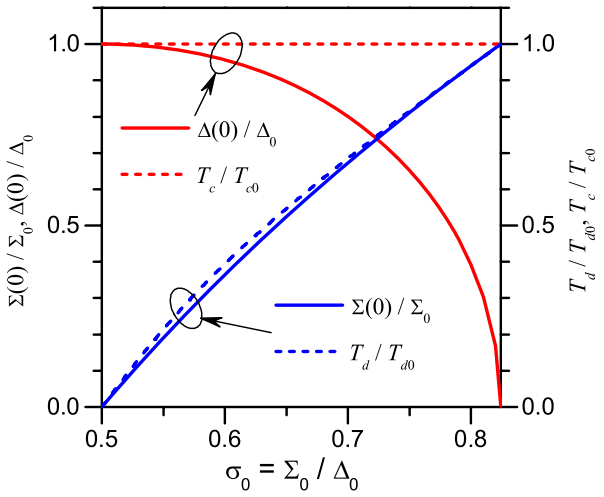

Figure 10. σ_0-dependences of the normalized order parameters at $T = 0$ and critical temperatures for complete CDW gapping.

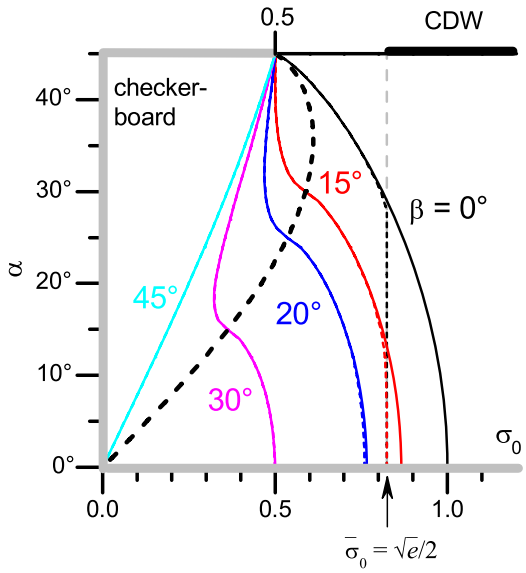

Figure 11. Phase diagrams for the checkerboard CDW configuration and various mismatch angles β. The dashed curve is the locus of the reentrance-collapse points (see the explanations in the text).

parameter value and the critical temperature: R_s for the s pairing and R_d for the d one. Those ratios are notably different in partially gapped d-wave superconductors [44]. The effect is even stronger for the complete dielectrization. Indeed, figure 9 demonstrates the effect readily in the whole range of σ_0. The calculated dependences can be explained by the examination of $\Sigma(T)$ and $\Delta(T)$ curves shown in figure 10. The patterns for the two order parameters differ substantially. Since $T_{c0} > T_{d0}$ in the whole relevant interval (15), the critical temperature $T_c = T_{c0}$ is not affected by the dielectric gapping. The parameter $\Delta(0)$ rapidly decreases with σ_0, since the upper part of the $\Delta(T)$-dependence in figure 7(b) is effectively cut away in comparison with typical theoretical or observed BCS-like curves, so a conventional increase of $\Delta(T)$ at low T is arrested for this set of problem parameters. At the same time, the $\Sigma(T)$-dependence 'collapses' with decreasing σ_0 almost uniformly and similarly to that of T_d. As a result (see figure 9), the ratio $\Delta(0)/T_c$ changes drastically with σ_0, whereas the ratio $\Sigma(0)/T_d$ varies insignificantly.

It is remarkable that in the degenerate case of complete dielectric gapping, $\Delta(0)/T_c$ is always smaller than the weak-coupling d-wave BCS value R_d, whereas for the partial CDW gapping observed in high-T_c oxides this ratio exceeds this weak-coupling limit according to both our theory [44] and the experiment [56]. The observed deviations in cuprates from the BCS value were treated earlier as the superconductivity-driven feedback suppression of the depairing by real thermal phonons [132] or as the specific property of the spin-fluctuation mechanism of Cooper pairing [24].

3.1.3. Non-zero-value mismatch angle between the CDW sector and the superconducting order parameter lobe: $\beta \neq 0$. Let us consider a more general case of the non-zero mismatch angle ($\beta \neq 0$; see figure 1) between the d-wave superconducting lobes and CDW sectors in the momentum space. As we indicated above, such a broken symmetry pattern might arise due to diverse intrinsic or extrinsic factors, which we do not specify in the framework of our phenomenological approach.

Figure 11 is a generalization of the phase diagram (figure 2) appropriate for cuprates to finite β-values. Solid and short-dashed curves denote the start-reentrance and end-reentrance boundaries, respectively, of the corresponding CDW-reentrance regions. The areas of pure BCS superconductivity and reentrance-free CDW superconductivity are positioned to the left of the end-reentrance boundary and to the right of the start-reentrance one, respectively (we do not use any hatching for clarity). Curves for $\beta = 0$ are equivalent to those depicted in figure 2, being plotted here for completeness.

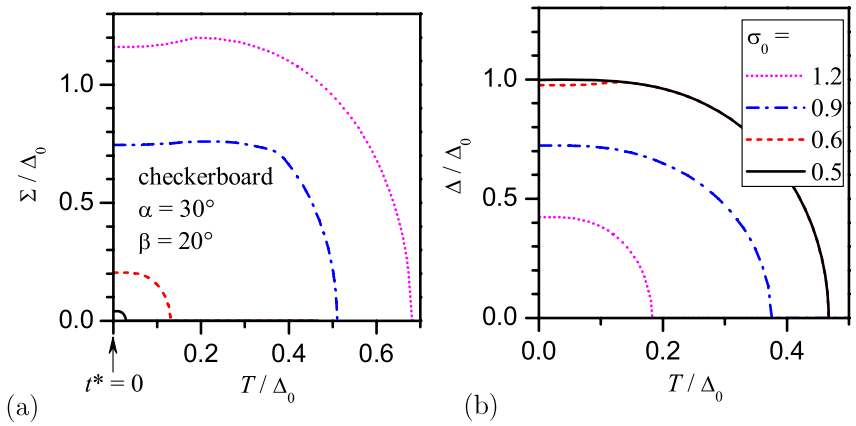

Figure 12. The same as figure 3 but for $\alpha = 30°$ and $\beta = 20°$.

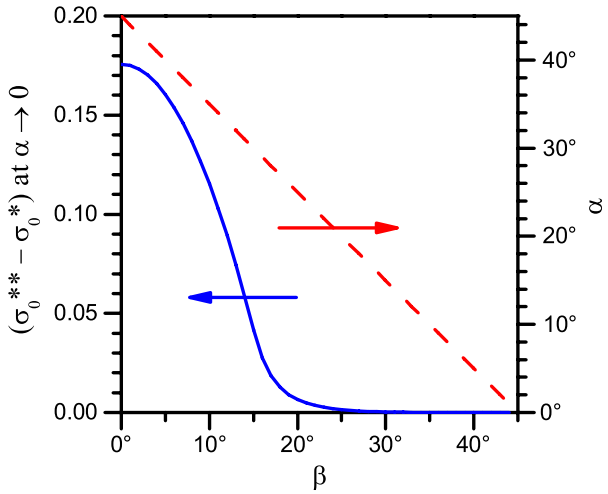

Figure 13. β-dependences of the base (solid curve) and the 'height' α (dashed curve) of the reentrance-collapse region (see figure 11).

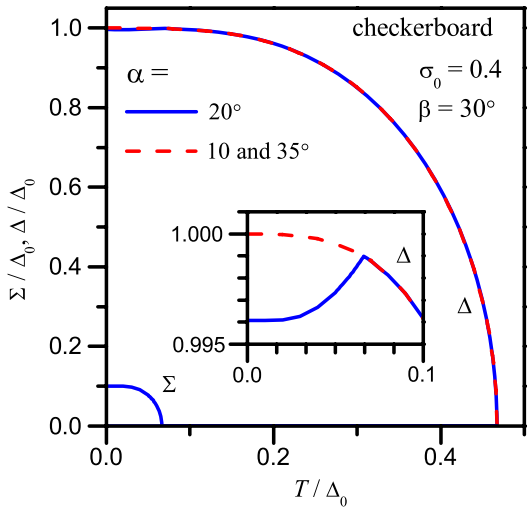

Figure 14. Normalized temperature dependences of Σ and Δ at various α-values (checkerboard configuration, $\sigma_0 = 0.4$, $\beta = 30°$). The scaled-up fragment of the figure is shown in the inset.

Our calculations show that, for every $\beta \neq 0$, there exists a specific upper limit for α, above which there is no reentrance region. In other words, the two boundaries of the CDW-reentrance region converge at $\alpha < \pi/4$, contrary to the situation for cuprates ($\beta = 0$). The locus of such points is shown in figure 11 by the bold dashed curve. The meaning of this curve is as follows. Figure 11 demonstrates that, for any β, the growth of α is accompanied by a shift of the collapse temperature T^* toward zero. This process can be better understood if we compare positions of $\Sigma(T)$ maxima in figures 4(a) and 5(a) in the 'precollapsing' regime. Finally, when the two boundaries of the CDW-reentrance region merge and the angle α grows further, $\Sigma(T)$ dependences always surround the coordinate origin collapsing to it as the value of σ_0 decreases (see figure 12(a)).

Hence, we may say that the region in the phase plane (σ_0, α) (see figure 11) between the bold dashed curve and the start-reentrance curve for $\beta = 0$ corresponds to those (σ_0, α)-pairs for which the reentrance of the dielectric order parameter may occur. This is a necessary condition but not a sufficient one for that event to take place. A point (σ_0, α) must also fall between the start-reentrance and end-reentrance boundaries for a selected mismatch angle β. From this point of view it is of interest to estimate the limits of the CDW-reentrance regions. For this purpose, let us calculate β-dependences of the base and height of those regions (see figure 13). By the base we mean a difference $\sigma_0^{**} - \sigma_0^*$ between the abscissas of the points on the (σ_0, α) phase plane, where the σ_0-axis intersects the start-reentrance, σ_0^{**}, and end-reentrance, σ_0^*, boundaries. The height is the ordinate α of the CDW-reentrance region maximum, where the two boundaries merge. Figure 13 attests to the region getting narrower very quickly as β increases. At the same time, its height seems to change strictly linearly. This means that any possibility of CDW-reentrance disappears when $\beta + \alpha \geq \pi/4$, i.e. when the CDW sector starts to overlap the superconducting node line on the FS.

The analysis of figure 11 shows that, at relatively large β, another kind of Σ-reentrance can take place (reentrance of kind II). Specifically, at a fixed σ_0, e.g., $\sigma_0 = 0.4$ (see figure 14), an increase of the opening angle α from zero at the beginning does not move the phase point out of the pure

SC region. Further increase of α transforms the system into a phase of the CDW superconductor, which persists within a certain α-interval. A subsequent growth of α restores the BCS superconducting state. Unfortunately, for this phenomenon to be observed, such a vertical trajectory must pass very close to the boundary between two relevant phases, so the maximal Σ-value achieved along this path is rather small.

In figure 14 one can find another interesting feature of the model associated with the mutual detrimental influence of superconductivity and CDWs. Namely, for a certain range of parameters the appearance of Σ invokes a dip in the $\Delta(T)$-dependence. The analogous effect of Δ on Σ was illustrated above in figure 7(b). However, in the latter case, the nonstandard behavior of the order parameter—its growth with T—could be demonstrated to avoid direct physical observation. Specifically, the thermodynamics of a CDW superconductor is not governed by each order parameter ($\Delta(T)$ and $\Sigma(T)$) separately, but by the effective energy gaps $\Delta(T)\cos 2\theta$ and $\sqrt{\Sigma^2(T)+\Delta^2(T)\cos^2 2\theta}$. Therefore, as was said above, the temperature growth of $\Sigma(T)$ on the nested FS sections could be compensated by a reduction of $\Delta(T)$, so the combined gap $\sqrt{\Sigma^2(T)+\Delta^2(T)\cos^2 2\theta}$ would remain monotonically decreasing. On the other hand, figure 14 evidences the possibility of the superconducting gap (!) $\Delta(T)\cos 2\theta$ reduction on the non-nested FS section as T drops within a certain interval. Nevertheless, this case should not be considered as counter-intuitive, because only the total free energy determined by the combined gaps over the whole FS is really essential. In this connection, note that this non-conventional $\Delta(T)$-dependence takes place at large α, when the fraction of non-nested FS is altogether small.

3.1.4. A particular case for $\beta = \pi/4$: d_{xy} symmetry of the superconducting order parameter. For the sake of definiteness we assume CDW sectors to be directed along p_x- and p_y-axes in the 2D momentum space (as in superconducting cuprates). At the same time, superconducting lobes are directed along diagonals of the Brillouin zone. This case corresponds to the d_{xy} orientation of the superconducting order parameter [15, 55, 96, 101–104]. As was shown in section 3.1.3, if $\alpha + \beta \geq \pi/4$, the Σ-reentrance of kind I is not observed, so the selected case $\beta = \pi/4$ always satisfies this condition. However, another interesting feature appears: Σ-sectors cover Δ-nodes. If both order parameters differ from zero the whole FS is gapped. Here, we would like to emphasize that non-zero gap coverage over the whole FS has to manifest itself macroscopically, e.g., it will lead to the exponential low-temperature asymptotics for a number of thermodynamic and transport properties of the CDW d superconductor. This issue will be treated in a separate work.

3.2. The unidirectional CDW configuration ($\Omega = \pi/2, N = 2$)

Let us consider now another CDW pattern in superconductors, with only one CDW family [51, 52, 58–61]. This configuration corresponds to the existence of dielectric gaps only in the hatched sectors on the FS (see figure 1). In terms of the relevant problem parameters, such a unidirectional CDW is described by the substitution $\Omega = \pi$ into formulas (8) and (11), or $N = 2$ into formula (11). Besides, the FS dielectric gapping angle α can now vary within the interval $[0, \pi/2]$. The range $[0, \pi/4]$ for the parameter β remains the same.

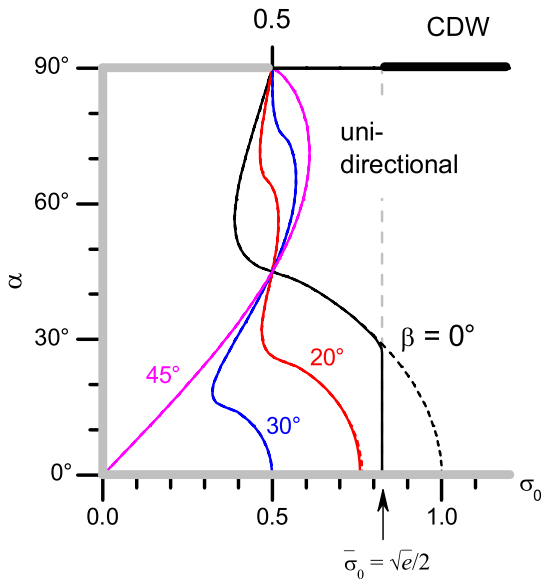

Figure 15. The same as figure 11, but for the unidirectional CDW configuration.

Before plotting the phase diagram for the unidirectional CDW superconductor, it is worth noting that the phase diagram characteristic features in the checkerboard case were obtained making use of only (A.1), which does not include N-dependent parameters. Therefore, those features remain the same, but the specific non-zero Σ- and Δ-values do differ for checkerboard and unidirectional CDW superconductors, because (11) is to be used for their calculation.

In particular, the lower ($0 \leq \alpha \leq \pi/4$) part of the phase diagram in the unidirectional case reproduces the phase diagram for the checkerboard CDWs; the upper plane ($\pi/4 \leq \alpha \leq \pi/2$) is new. The set of phase diagrams for various β-values is depicted in figure 15. The figure demonstrates that no regions with T-driven CDW-reentrance exist at $\alpha \geq \pi/4$. Besides, for any β (including the most important 'cuprate' value $\beta = 0$), we can select such σ_0 that the variation of α would reveal the effect of Σ-reentrance of kind II.

The influence of the number of Σ-sectors on the magnitude of the order parameters is illustrated in figure 16. Here, three scenarios are presented: one (panel (a)) without any reentrance, i.e. the phase point is in the SC + CDW region, and other two with the reentrance in the cases $\sigma_0 > \bar{\sigma}_0$ (panel (b)) and $\sigma_0 < \bar{\sigma}_0$ (panel (c)). We can see that the value of T_c changes with Ω in the (a) and (b) panels. This is not at all strange. Indeed, more Σ-sectors with identical opening angles correspond to a higher degree of effective FS dielectric gapping, which suppresses T_c [44]. Mathematically, it follows from the fact that T_c is determined from (8), which includes the parameter Ω. The reciprocally detrimental effect of superconductivity and CDWs is also confirmed by the relationships between the order parameter magnitudes: in

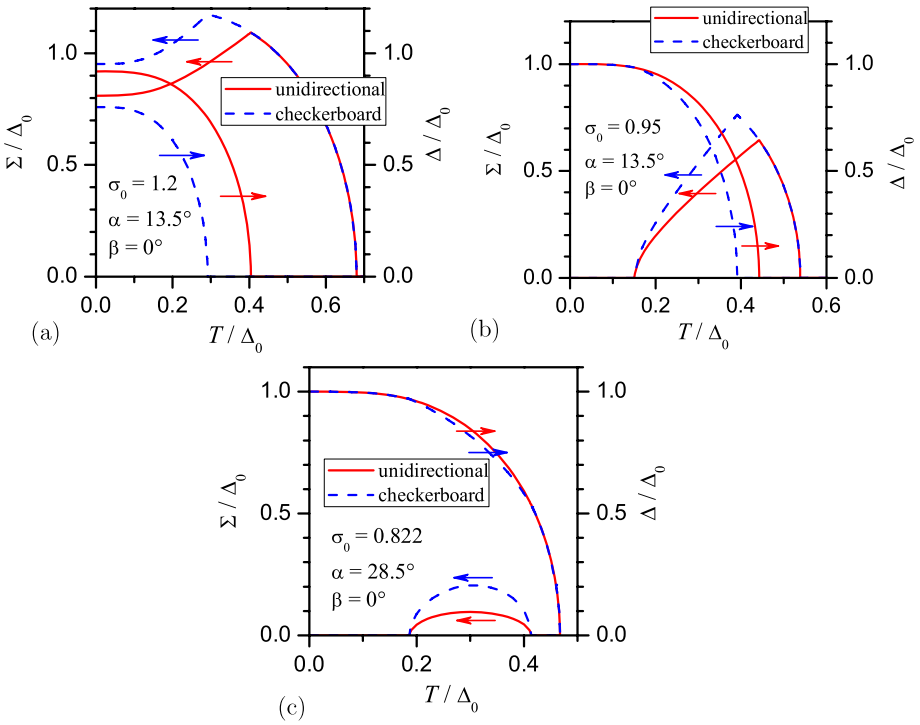

Figure 16. Comparison of the normalized $\Sigma(T)$- and $\Delta(T)$-dependences in the unidirectional and checkerboard configurations for various sets of system parameters.

the checkerboard configuration, when the role of CDWs is higher, Σ-values are larger and Δ-values smaller than their counterparts in the unidirectional case. Additionally, the figure indicates that the phase diagram (σ_0, α)—to be more accurate, the separatrices in the (σ_0, α) plane confining pure SC, SC + CDW, and CDW-reentrance phases—are independent of the Σ-sector number N at $\alpha \leq \pi/4$.

Of course, the gap roses do change, sometimes drastically. In figures 17(a)–(c), the evolution of gap roses is exhibited for each set of problem parameters illustrated in figures 16 ((a)–(c), respectively). The figures demonstrate that the change of Σ-sector geometry results in visibly non-similar angular gap patterns only when magnitudes of Σ and Δ are comparable. Otherwise, the two roses are indistinguishable. For instance, diagrams at $t = 0.1$ and 0.45 in the checkerboard geometry are identical to their counterparts in the unidirectional one, because $\Sigma(t = 0.1) = \Sigma(t = 0.45) = 0$. At $t = 0.3$, as stems from figure 16(c), $\Sigma(t) \neq 0$. But even in this case the difference between order parameter magnitudes in different geometries and the loss of 90°-rotation symmetry for the gap pattern are insufficient to discriminate between the checkerboard and unidirectional Σ-configurations. In particular, the gap maximum in figure 16(a) equals 0.844, whereas the two maxima in figure 16(b) are 0.852 and 0.847 for 0°- and 90°-directions, respectively.

4. Conclusions

The phase diagrams constructed and various dependences of relevant quantities describing d-wave superconducting, CDW + d-wave superconducting, and reentrant CDW + d-wave superconducting phases reveal a diverse picture, which is much richer than its counterpart for CDW s-wave superconductors [22]. In particular, we can draw a conclusion that the pseudogap (CDW gap, according to our model) in cuprates may be difficult to detect due to its reentrant character. Hence, the calculated phase diagrams would be of help in giving an important overall insight and even quantitative benchmarks. The latter is no surprise, since the control parameter α is a measurable property [40, 114–116], independent of fine details of the electron spectrum and a cornerstone of the adopted phenomenological scenario.

In particular, our isotherm maps shown in figures B.2(a) and D.1(a) and corresponding to the cuprate case ($\beta = 0$) clearly demonstrate how swiftly T_c falls with the growth of the CDW sector α, i.e. while going from overdoped to the underdoped samples. Such a link between doping, on the one hand, and T_c and α, on the other hand, was observed, e.g., in the oxides $Bi_2Sr_{2-x}La_xCuO_{6+\delta}$ and $Bi_2Sr_2CaCu_2O_{8+\delta}$ [116]. We emphasize that these relationships exist whatever the number of CDW sectors N, although there are quantitative distinctions between the checkerboard and unidirectional cases.

We have shown that the ratio $\Delta(0)/T_c$ in CDW superconductors may differ substantially from its weak-coupling value for the parent d-wave superconductor [98, 99] even if the Cooper pairing is assumed to be a weak-coupling one. Note that strong Coulomb correlations between quasiparticles (the Mott–Hubbard picture) [5, 24, 25] are also taken into account here although implicitly by dividing the FS into nested and non-nested sections (hot and cold spots,

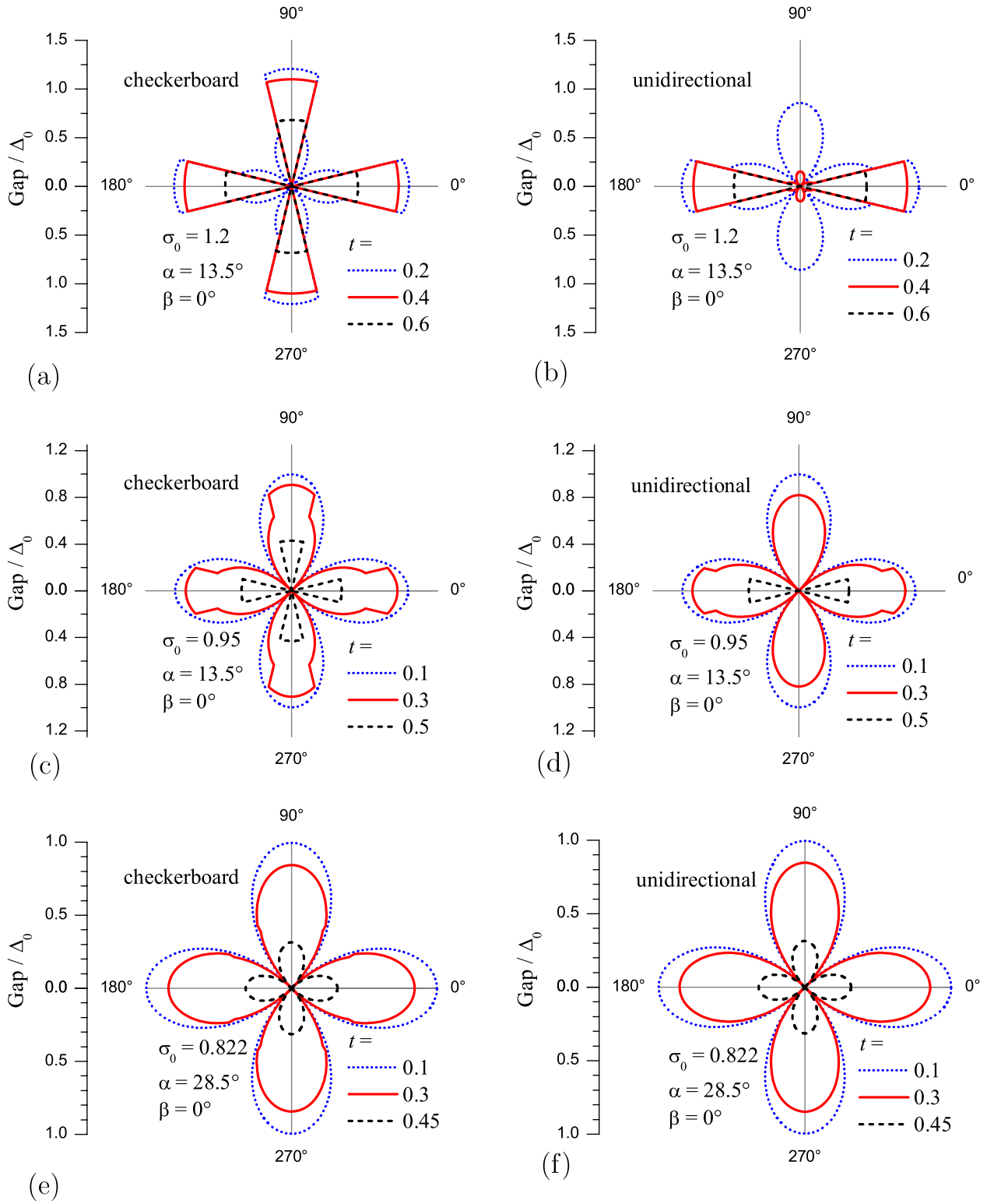

Figure 17. Comparison of temperature evolution of the gap roses in the unidirectional and checkerboard configurations for various sets of system parameters.

respectively). Moreover, this speculative splitting is supported by the experiment [2, 9, 10, 40, 114–116]. We guess that the interplay between order parameters of other natures but also possessing different symmetries may lead to reentrant phenomena for the weaker order parameter, similar to that found here for $\Sigma(T)$ and $\Sigma(\alpha)$. Perhaps some hidden interplay of this kind taking place in $Bi(Pb)_2Sr_2Ca(Tb)Cu_2O_{8+\delta}$ results in the nonmonotonic T-behavior of the pseudogap there [2].

The 'gap roses' depicted show that ARPES angular diagrams represent peculiar combinations of order parameters

as angle-dependent combined gaps rather than each order parameter separately (see also recent experimental data in [4, 133], as well as the analysis of photoexcited quasiparticle relaxation dynamics in [134]). The same is true for tunnel and point-contact measurements, where certain tricks are used to single out each order parameter contribution [42, 116, 135, 136]. Therefore, the proportionality found between the apparent gap and temperature T_{pg}, below which the pseudogap starts to manifest itself [137], does not mean that the observed gap is the superconducting one, Δ.

Unidirectional CDWs interact with d-wave superconductivity similarly to checkerboard ones, although externally driven switching between the patterns may lead to conspicuous differences between resulting ARPES or tunnel spectra. As for a mismatch ($\beta \neq 0$) between $\Delta(\theta)$ and $\Sigma(\theta)$ maxima, it substantially changes phase diagrams. The effect would have strongly manifested itself especially for d_{xy} superconductivity if a corresponding material had been found.

Acknowledgments

AMG and AIV are grateful to Kasa im Józefa Mianowskiego, Fundacja na Rzecz Nauki Polskej, and Fundacja Zygmunta Zaleskiego for the financial support of their visits to Warsaw. MSL is grateful to the Ministry of Science and Informatics of Poland (grant no. 202-204-234). The work of AMG, AIV, MSL, and HS was partially supported by the Project N 23 of the 2009–2011 Scientific Cooperation Agreement between Poland and Ukraine. AMG wishes to express great appreciation of the 2010 Visitors Program of the Max Planck Institute for the Physics of Complex Systems (Dresden, Germany). We greatly appreciated the interesting discussions on high-T_c superconductivity and charge-density-wave instability with S Borisenko (Dresden), D Evtushinsky (Dresden), D Inosov (Stuttgart), B Keimer (Stuttgart), J Köhler (Stuttgart), A Kordyuk (Dresden), D Manske (Stuttgart), and A Menushenkov (Moscow).

Appendix A. The phase diagram at $\beta = 0$; details

Let us rewrite (10) (the σ-equation) in a different form:

$$F_\sigma(\delta, \sigma, t, \alpha, \beta) = -\ln\sigma_0, \tag{A.1}$$

where

$$F_\sigma(\delta, \sigma, t, \alpha, \beta) = \frac{1}{2\alpha}\int_{-\alpha}^{\alpha} I_M\left(\sqrt{\sigma^2 + \delta^2\cos^2 2(\beta+\theta)}, t, 1\right)\mathrm{d}\theta, \tag{A.2}$$

so that all the problem parameters and variables, but σ_0, are contained in its left-hand side, whereas the right-hand side includes only σ_0. The reentrance-start condition, (14), follows immediately from (A.1) if one puts $t = 0$, $\sigma(t = 0) = 0$, and $\delta(t = 0) = 1$ there. But the content of this equation turns out to be much richer.

Equation (A.1) describes, together with (11) (the δ-equation), the temperature dependences of both order parameters in the range of their coexistence. At the same time, it can alone describe the dependence $\sigma(t)$ at $t > t_c$ if t_c is lower than t_d, i.e. in the interval $t_c < t < t_d$, where $\delta = 0$. The point of our interest is the coexistence interval. The most interesting situation arises when the set of parameters admits the reentrance regime for the dielectric order parameter σ. In this case, the system of (A.1) and the δ-equation (11) has two roots t_r and t_d in the temperature interval $0 < t < t_{c0}$: $0 < t_r < t_d < t_{c0}$. At the end points t_r and t_d of the coexistence region, $\sigma(t_r) = \sigma(t_d) = 0$, whereas δ acquires values in accordance with the dependence $\delta = M\ddot{u}_d(1, t)$.

Let us consider the auxiliary function

$$F_\sigma(t, \alpha, \beta) = F_\sigma(\delta = M\ddot{u}_d(1, t), \sigma = 0, t, \alpha, \beta) = \frac{1}{2\alpha}\int_{-\alpha}^{\alpha} I_M(M\ddot{u}_d(1, t)\cos 2(\beta+\theta), t, 1)\,\mathrm{d}\theta. \tag{A.3}$$

This function describes the behavior of all peculiarities connected with dielectric gapping, including its collapse. This is the case because functions (A.2) and (A.3) coincide at the points t_r and t_d, where $\sigma = 0$. At $t = t_{c0}$, the function $F_\sigma(t, \alpha, \beta)$ has a cusp, associated with a square-root peculiarity of the function $M\ddot{u}_d(1, t)$ at $t \to t_{c0} - 0$. Moreover, in accordance with our agreement that $M\ddot{u}_d(1, t \geq t_{c0}) = 0$, we can extend this function to the right from this point, where it becomes independent of α and β. It is easy to calculate that

$$F_\sigma(t \geq t_{c0}, \alpha, \beta) = \ln\frac{\gamma}{\pi t}. \tag{A.4}$$

Now, to determine peculiarities connected with the dielectric gapping, it is enough to solve the equation

$$F_\sigma(t, \alpha, \beta) = -\ln\sigma_0, \tag{A.5}$$

which is a much simpler task than the solution of the system of σ- and δ-equations. (However, to obtain the specific $\Sigma(T)$- and $\Delta(T)$-profiles in the coexistence interval, that system of equations has to be solved of course.) The task becomes even easier because the variation of parameter σ_0 in (A.5) does not deform the $F_\sigma(t, \alpha, \beta)$-profile, but is reduced to the shift of the latter by the value $\ln\sigma_0$ along the ordinate axis, or equivalently, which is a literal interpretation of (A.5), to monitoring where the function $F_\sigma(t, \alpha, \beta)$ equals $-\ln\sigma_0$.

In figure A.1, the family of functions $F_\sigma(t, \alpha, \beta = 0°)$ for various α-values are depicted. The maximum of each curve, which, as we shall see soon, corresponds to the reentrance-collapse, is marked by a circle. The point located at $t = t_{c0}$, where all the left-hand branches converge and which is a maximum common to a number of curves, is marked by a hollow circle. The ordinate of this point can be easily determined from (A.4) to equal $-\ln\tilde{\sigma}_0$.

Let us illustrate how it all works. In section 3.1.1, we analyzed the evolution of $\sigma(t)$-dependences with varying σ_0 at $\beta = 0$ and $\alpha = 13.5°$ (figure 3). The corresponding function $F_\sigma(t, \alpha = 13.5°, \beta = 0°)$ is depicted in figure A.2. At large σ_0, it has a single root t_d, which, according to (A.4) and (A.5), equals $t_d = \sigma_0/R_s$ (a pure CDW metal). The phase point is in the SC + CDW region (figure 2), and the temperature dependences $\Sigma(T)$ and $\Delta(T)$ behave like those depicted by $\sigma_0 = 1.2$-curves in figure 3. At $\sigma_0^{**} \approx 0.9623$, the

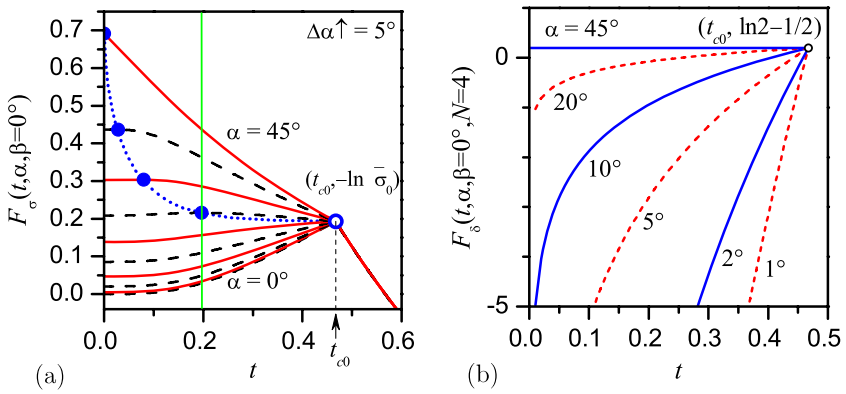

Figure A.1. Variation with α of auxiliary (a) $F_\sigma(t)$-functions and (b) $F_\delta(t)$-functions for σ-equations (10) and δ-equations (11), respectively, at $\beta = 0°$ (see explanations in the text).

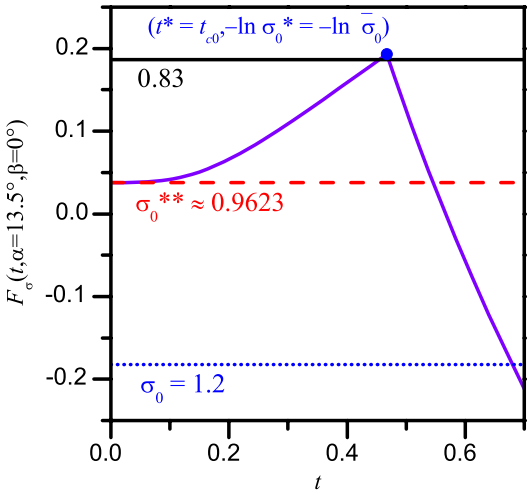

Figure A.2. Illustration of how the auxiliary function $F_\sigma(t, \alpha = 13.5°, \beta = 0°)$ is used to obtain the $t_d(\sigma_0)$- and $t_r(\sigma_0)$-dependences, while moving along the $\alpha = 13.5°$-path in the phase diagram depicted in figure 2. The specific σ_0-values are the same as in figure 3.

phase point crosses the reentrance-start boundary (figure 2), and the t_r point emerges starting from the value $t_r = 0$ (figure A.2). The corresponding σ_0^{**}-value is determined by the ordinate y of the point where the plot of the function $F_\sigma(t, \alpha, \beta)$ intersects the ordinate axis: $y = -\ln\sigma_0^{**}$. The critical temperature t_d continues to be $t_d = \sigma_0/R_s$, according to (A.4) and (A.5). The points t_r and t_d come closer at higher σ_0, so the reentrance interval becomes narrower (see the $\sigma_0 = 0.83$-curves in figure A.2). Finally, at $\sigma_0 = \bar{\sigma}_0$ (the coordinate of the cusp maximum in figure A.2), the two dielectric critical temperatures converge, and the $\Sigma(T)$-dome collapses. At that moment, the phase point crosses the reentrance-collapse boundary in the phase diagram (figure 2), finding itself in the region of pure BCS superconductor, which stretches down to $\sigma_0 = 0$.

For other α-values close enough to 13.5°, the order parameter behavior is qualitatively the same. Since the cusp-like maximum at $t = t_{c0}$ remains fixed, the reentrance-collapse σ_0^* will also not change. It corresponds to the strictly vertical motion along the reentrance-collapse boundary (figure 2) at small enough α. At the same time, as can be seen from figure A.1, the σ_0^{**}-value, which is associated by formula (A.5) with the value $F_\sigma(t = 0, \alpha, 0°)$, varies with α. Thus, we obtain an explanation for the fact noted in section 3.1.1 that the reentrance interval $\sigma_0^{**} - \sigma_0^*$ narrows at small α owing to the shift of σ_0^{**} only. The collapse temperature t^* also does not change, and we obtain a wide plateau in the dependence $t^*(\alpha)$ (see curve $\beta = 0°$ in figure 6).

However, such a vertical motion of the collapse point in the phase diagram keeping the collapse temperature constant cannot be preserved within the whole range of α- or μ-change. Indeed, in this case, the reentrance-collapse boundary would have intersected the reentrance-start separatrix, where $t_r = 0$. At the same time, at the vertical path of the collapse point, one has $t_r = t_d = t_{c0} \neq 0$. This controversy means that the geometrical locus of collapse points must sooner or later deviate from its vertical part, as can be seen in the inset of figure 2. According to figure A.1, the value of α_{lim}, when the deviation starts, is determined by the equation

$$\left[\frac{dF_\sigma(t, \alpha, \beta)}{dt}\right]_{t \to t_{c0}-0} = 0. \qquad \text{(A.6)}$$

At larger α, the point of left-branch convergence is no longer the maximum. Every $F_\sigma(t, \alpha, \beta)$-dependence at $\alpha > \alpha_{lim}$ has its own maximum with specific coordinates (see the circles in figure A.1). Therefore, the collapse coordinates t^* and σ_0^* are also no longer fixed.

In figure A.3, the plot of the function $F_\sigma(t, \alpha = 28.5°, \beta = 0°)$ is depicted. It is enough to analyze in detail the evolution of peculiarities in the corresponding $\Sigma(T)$-dependences shown in figure 4(a). Since the cusp-like peculiarity is no longer the maximum, a new feature appears: every $\Sigma(T)$-dome obtained at $\sigma_0 < \bar{\sigma}_0$ is located within the superconducting interval: $0 < t_r < t_d < t_c = t_{c0}$, which is illustrated in figure 4(a). The reentrance interval $[\sigma_0^*, \sigma_0^{**}]$ becomes narrower (figure 2), and the collapse temperature t^* decreases (figure 6).

Figure A.1 also demonstrates (see the dash–dotted curve) that the locus of maximum points approaches the ordinate axis, but reaches it only at $\alpha = \frac{\pi}{4}$. This means that the

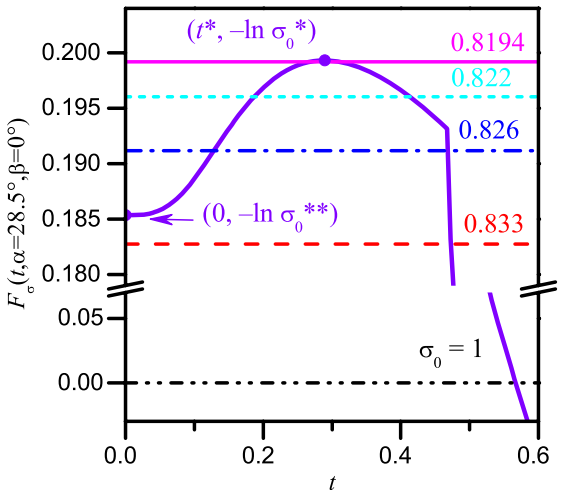

Figure A.3. The usage of the auxiliary function $F_\sigma(t, \alpha = 28.5°, \beta = 0°)$. The specific σ_0-values are the same as in figure 4.

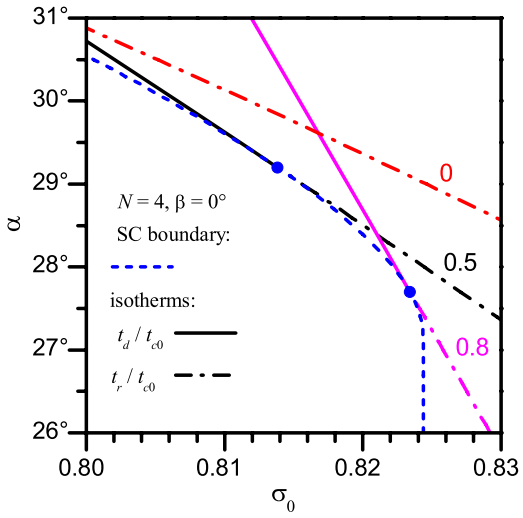

Figure B.1. Illustration of the smooth transformation between t_d- and t_r-isotherm branches at the SC-phase boundary. Examples are shown for $t_d = t_r = 0.5t_{c0}$ and $0.8t_{c0}$. The $t_r = 0$-branch (the reentrance-start boundary) has no $t_d = 0$-counterpart.

difference between the maximum and intersection point ordinates ($-\ln\sigma_0^*$ and $-\ln\sigma_0^{**}$, respectively) is zero only in this limiting case, which corresponds to complete FS dielectric gapping. But this fact is equivalent to the statement that the reentrance interval $[\sigma_0^*, \sigma_0^{**}]$ is preserved across the whole phase plane, though becoming very narrow at large $\alpha \to \frac{\pi}{4}$. It also means that the collapse temperature t^* differs from zero along the whole reentrance-collapse boundary up to $\alpha = \frac{\pi}{4}$, exclusively. Another conclusion is that the phase diagram for a hypothetical totally dielectrized CDW d superconductor has no reentrance regions for the dielectric order parameter $\Sigma(T)$; note that the mismatch angle β is irrelevant in this case.

Appendix B. Isotherms at $\beta = 0$

The content of the function $F_\sigma(t, \alpha, \beta)$ introduced in appendix A is not confined to the issues discussed there. Indeed, according to definition (A.3), this function provides adequate information concerning events that occur at $\sigma = 0$. In particular, it also allows one to plot isotherms for the characteristic temperatures t_r and t_d on the phase plane α–σ_0. Mathematically, this task is reduced to the solution of (A.5) at certain fixed β and t. But one has to be careful in order not to confuse t_r and t_d. Let us consider again the family of $F_\sigma(t, \alpha, \beta = 0°)$-functions (figure A.1(a)). The point of intersection of a representative solid line at, say, $t \approx 0.2$ with any curve $F_\sigma(t, \alpha, \beta = 0°)$ gives a solution with either $t_r \approx 0.2$ or $t_d \approx 0.2$ and a corresponding point on the phase diagram figure 2. But, as we found out in appendix A, for any curve, the section to the left from the relevant maximum is the locus of σ-reentrance temperatures (in particular, the ordinates of intersection points between the curves concerned with the ordinate axis describe the reentrance-start boundary). On the other hand, the section to the right from the maximum is the locus of the critical dielectric temperatures. Therefore, tracing the representative point along the straight line $t \approx 0.2$ in figure A.1(a), one will obtain $t_r \approx 0.2$ if the intersection point belongs to the left branch, or $t_d \approx 0.2$ if it belongs to the right branch of the same curve described by (A.5). At the same time, the $\beta = 0°$-curve in figure 6 attests to any pair of isotherms (t_d, t_r) within the temperature interval $(0, t_{c0})$ having only one point of intersection with the reentrance-collapse boundary. This point connects the two isotherms smoothly.

Figure B.1 illustrates a crossover of t_d-isotherms into corresponding t_r-isotherms for two normalized temperatures. One can see that any 'combined' t_d–t_r-isotherm is tangent to the collapse boundary locus.

The application of the auxiliary function $F_\sigma(t, \alpha, \beta)$ together with (A.5) proved to be extremely useful for the analysis of various features in the behavior of the dielectric order parameter Σ on the phase plane. A reasonable question arises as to whether anything similar can be done with (11). Below we show that this is feasible, the role of Σ and Δ being reversed. Note that when we put $\delta = 0$ and $\sigma(t) = M\ddot{u}_s(\sigma_0, t)$ into the δ-equation (11), we introduce the parameter σ_0, thus making possible the analysis of relevant curves on the phase plane σ_0–α. Moreover, since $\delta = 0$, the cosine dependence in the combination $\delta\cos 2\theta$ disappears altogether, and the integrals can be reduced to elementary functions. Hence, an analogue of (A.5), but deduced from (11), looks quite simple:

$$F_\delta(t, \alpha, \beta, N) = -\ln\sigma_0, \tag{B.1}$$

where

$$F_\delta(t, \alpha, \beta, N) = \frac{\left(\frac{\pi}{N} - \zeta(\alpha, \beta)\right)\ln\frac{\pi t}{\gamma} + \frac{\pi}{N}(\ln 2 - \frac{1}{2})}{\zeta(\alpha, \beta)} \tag{B.2}$$

with

$$\zeta(\alpha, \beta) = \alpha + \tfrac{1}{4}\sin 4\alpha\cos 4\beta.$$

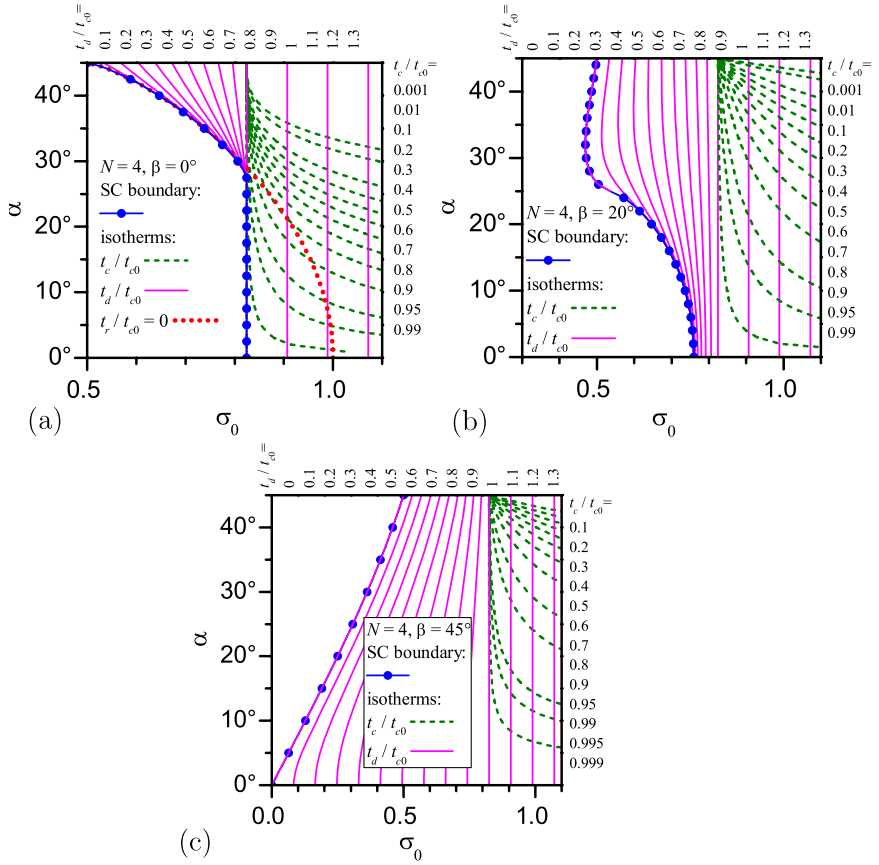

Figure B.2. Normalized $T_{\rm d}$- and $T_{\rm c}$-isotherms on the phase plane in the checkerboard CDW configuration for a few β-values.

However, this equation is valid only for $t < t_{\rm d0}$. At $t \geq t_{\rm d0}$, the whole (11) with the inputs $\delta = 0$ and $\sigma(t) = M\ddot{u}_{\rm s}(\sigma_0, t)$ looks like $t = t_{\rm c0}$, which is quite natural (see below). In figure A.1(b), a family of $F_\delta(t, \alpha, \beta = 0°, N = 4)$-dependences for various α-values is depicted. The figure demonstrates that every curve is smooth and monotonic, so the possibility of a Δ-reentrance phenomenon is out of the question, and (B.1) serves as the basis for determining a single superconducting critical temperature $t_{\rm c}$.

Before plotting the critical temperature isotherms for the CDW superconductor, it would be instructive to clarify what is observed for its parent phases: a CDW metal and a BCS superconductor. It is convenient here to carry out the normalization with respect to the 'parent' superconducting critical temperature $T_{\rm c0}$. Then, for the parent BCS superconductor, the whole phase plane—see section 3.1.1—is a single critical temperature isotherm $T_{\rm c} = T_{\rm c0}$. The critical temperature for the parent CDW metal is $T_{\rm d0} = \Sigma_0/R^{\rm s}_{\rm BCS}$. Therefore, critical temperature isotherms of the parent CDW metal, $\frac{T_{\rm d0}}{T_{\rm c0}} = \sigma_0 \frac{R^{\rm d}_{\rm BCS}}{R^{\rm s}_{\rm BCS}} = \frac{\sigma_0}{\bar{\sigma}_0}$, are straight lines oriented in parallel to the α-axis. At $\sigma_0 = \bar{\sigma}_0$, the critical temperatures are equal, $T_{\rm d0} = T_{\rm c0}$, being lower than $T_{\rm c0}$ to the left from the $\sigma_0 = \bar{\sigma}_0$-line and higher to the right.

It is clear that, when we consider the CDW superconductor, the higher 'parent' critical temperature determines the actual—higher!—critical temperature of the corresponding order parameter. Hence, if $T_{\rm d0} \neq T_{\rm c0}$, a temperature interval exists in the vicinity of higher critical temperature, where only one kind of gapping takes place. Moreover, since the two pairings are detrimental to each other, a stronger pairing inhibits its competitor and shifts the corresponding actual critical temperature toward zero, so the observed difference between actual critical temperatures $|T_{\rm d} - T_{\rm c}|$ is always larger than its counterpart between 'parent' parameters $|T_{\rm d0} - T_{\rm c0}|$. Hence, the critical temperature isotherms corresponding to the phenomenon with a lower critical temperature become distorted in comparison with the 'parent' isotherms.

Thus, if we consider isotherm maps for critical temperatures of the CDW superconductor normalized by $T_{\rm c0}$, the map for superconducting critical temperatures $T_{\rm c}/T_{\rm c0}$ will always include the undistorted area (with $T_{\rm c}/T_{\rm c0} = 1$) to the left from the line $\sigma_0 = \bar{\sigma}_0$ (this plane is a visual illustration of the above mentioned transformation of (B.1) into the equality $t_{\rm c} = t_{\rm c0}$ at $t \geq t_{\rm d0}$). At the same time, the map for the dielectric critical temperature $T_{\rm d}/T_{\rm c0}$ will always include the undistorted straight-line isotherms to the right from this separatrix.

One sees that to the right from the vertical separatrix $\sigma_0 = \bar{\sigma}_0$, where $T_{\rm c0} < T_{\rm d0}$, CDWs appear at higher T than superconductivity and reduce $T_{\rm c}$. Naturally, such a detrimental influence is more effective at high extent of the FS dielectric gapping μ (large α), and the magnitudes of $T_{\rm c}$ gradients, $\mathrm{d}T_{\rm c}/\mathrm{d}\sigma_0$, are very large here. Nevertheless, the dependences $T_{\rm c}(\sigma_0)$ are continuous along any path, except for the case

of complete FS dielectric gapping. At the same time, the dielectric critical temperature T_d abruptly vanishes at the reentrance-collapse curve. The reason is that $T_d \approx T^*$ in the vicinity of this separatrix, and $T^* = 0$ only at $\alpha = \pi/4$ (see the curve for $\beta = 0$ in figure 6). Therefore, it turns out that at $\beta = 0$, the critical temperature of the dielectric gapping can be arbitrarily small only in the vicinity of the complete dielectric gapping case ($\alpha = \pi/4$).

To summarize, at $\beta = 0$, the dependences $T_c(\Sigma_0)$ are continuous, whereas the dependences $T_d(\Sigma_0)$ are discontinuous at any degree of the FS dielectric gapping, except for the case of complete gapping when the situation is inverse—$T_c(\Sigma_0)$ is a discontinuous and $T_d(\Sigma_0)$ a continuous function (see figure 10). We also emphasize that any T_d-isotherm with $t_d/t_{c0} < 1$ does not approach the reentrance-collapse curve asymptotically. It terminates at their corresponding intersection point, which can be easily inferred from figure 6.

Appendix C. The phase diagram at $\beta \neq 0$; details

It is clear from general reasoning supported by calculations (see figure 11) that the scenario where the function $F_\sigma(t, \alpha, \beta = 0°)$ for low α has a cusp-like maximum at $t = t_{c0}$ is valid not only for $\beta = 0°$, but also in a certain adjacent β-interval. At the same time, for large enough $\beta \neq 0$ the function $F_\sigma(t, \alpha, \beta)$ becomes monotonic—and so its maximum shifts to $t = 0$—above a certain $\alpha < \pi/4$. We would like to illustrate the situation where the cusp-like feature is no longer the maximum. In figure C.1, we present the family of F_σ- and F_δ-curves—analogues of figures A.1—but for the case $\beta = 20°$ (see the corresponding curve in figure 11). Figure C.1(a) demonstrates that the collapse temperature t^* (the abscissa of the maximum point) varies in a narrower interval than it did at $\beta = 0°$ and vanishes at $\alpha = 25°$. More detailed information concerning the dependences $t^*(\alpha)$ for $\beta = 20°$ and other β-values can be obtained from figure 6. All of this means that T_d becomes a continuous function of σ_0 at high enough degrees of the FS dielectric gapping ($\alpha \geq \frac{\pi}{4} - \beta$). At $\alpha < \frac{\pi}{4} - \beta$, the dependence $T_d(\sigma_0)$ retains a discontinuity at the separatrix (see appendix B). But, at $\alpha > 25°$, the $T_d(\sigma_0)$-dependence is continuous, which means that the $\Sigma(T)$-profile collapses to the coordinate origin with reducing σ_0, as is demonstrated in figure 12. On the other hand, a comparison between $F_\delta(t)$-profiles (figures A.1(b) and C.1(b)) evidences that the intervals between the curves at a fixed t become larger, which means that the relief formed by t_c-isotherms of the phase plane becomes more gentle.

Figure B.2(b) exhibits the contour maps for the normalized dielectric and superconducting critical temperatures in the case $\beta = 20°$. It is worth noting that, in accordance with the foregoing, the $t_d = 0$-isotherms appear at $\beta \neq 0°$. Those isotherms as expected lie along the boundaries of the corresponding pure superconducting regions. At the same time, they occupy only a certain section of this separatrix. In the case analyzed ($\beta = 20°$), this section is confined within the range $\alpha = 25°$–$45°$. We also emphasize that t_d-isotherms with $t_d < t^* R_d$ do not continue to the lower boundary of the phase diagram but terminate at the corresponding points on the separatrix, which can be easily determined from figure 6. The corresponding continuation of every t_d-isotherm after the latter arrives at the separatrix—they are described by the same form, (A.5)—is a t_r-isotherm. We do not present even the $t_r = 0$-isotherm here, as was done in figure B.2(a) for the case $\beta = 0°$, because, as figure 13 shows, the maximal σ_0-distance between this isotherm and the reentrance-collapse boundary, which is attained at $\alpha \to 0°$, is about 0.01, so the two curves are almost indistinguishable on this scale (the other t_r-isotherms are even closer to the reentrance-collapse boundary). The figure demonstrates that the t_c-profiles to the left from the $t_c = t_d$-line became less steep in comparison with the case $\beta = 0°$ (appendix B), although their character does not change in principle. The variations of t_d-profiles are more pronounced. For the chosen specific value $\beta = 20°$, the collapse temperature is $t^* \approx 0.174$ (it is the ordinate of $\beta = 20°$-curve at $\alpha = 0°$ in figure 6).

Figure B.2(c) demonstrates an analogous critical temperature isotherm map in the case $\beta = 45°$ (the d_{xy} Cooper pairing). The t_c-profile is even less steep, any t_d-isotherm extends across the whole phase plane, and the whole boundary of the non-dielectrized superconducting region is the $t_d = 0$-isotherm.

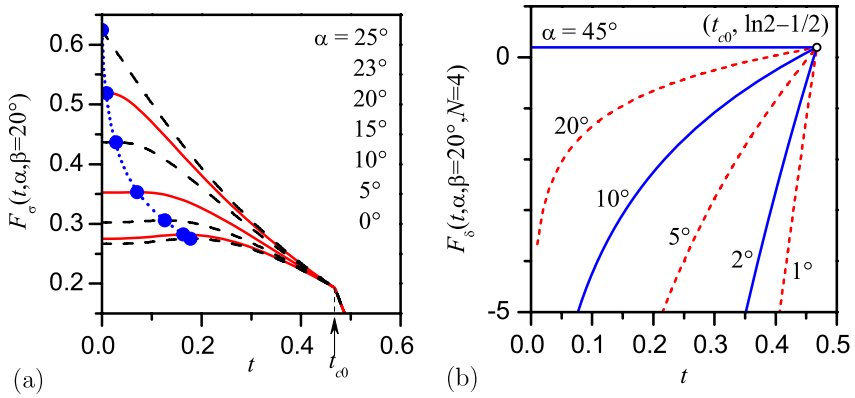

Figure C.1. The same as figure A.1, but at $\beta = 20°$.

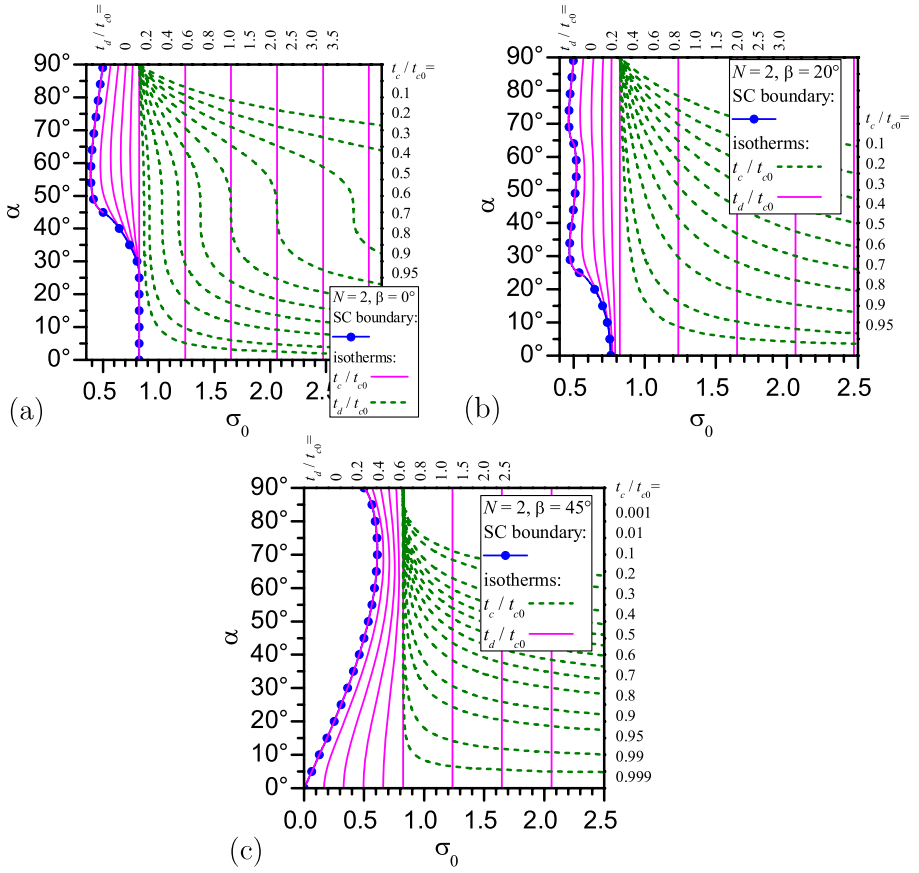

Figure D.1. The same as figure B.2, but in the unidirectional CDW configuration.

Appendix D. Contour maps for critical temperatures for the unidirectional CDW configuration ($N = 2$)

In figures D.1(a)–(c), the isotherms of the critical temperatures t_d and t_c are depicted for the case of a unidirectional CDW configuration. As for the t_d-isotherms, their lower segments ($\alpha < 45°$) are precise duplications of isotherms depicted in appendices B and C. This is true, because the generating function $F_\sigma(t, \alpha, \beta)$ (see formula (A.3)) does not depend on the parameter N, being equal in the two geometries concerned at $\alpha < 45°$. The special interesting feature is that the case $\alpha = 45°$ at $N = 4$ and the case $\alpha = 90°$ at $N = 2$ are equivalent: they both correspond to the completely dielectrically gapped FS. Therefore, σ_0 values for any t_d-isotherm map are the same in pairs at $\alpha = 45°$ and 90°. Points of low t_d-isotherms at $\alpha > \frac{\pi}{4}$ constitute an important particular case. The continuous behavior of the boundary, defined by (14), and adjacent t_d-isotherms at $\alpha \to \frac{\pi}{4} - 0$ dictates that, at $\alpha > \frac{\pi}{4}$, there must be at least one segment convex to the left. Therefore, when the representative point moves along a path $\sigma_0 = \text{const}$ with a varying extent of the FS dielectric gapping (this can be realized by doping the relevant high-T_c oxide), a CDWs state ($\Sigma \neq 0$) will appear and vanish again (the reentrance behavior of kind II, according to our terminology).

Formula (B.2), responsible for the behavior of the t_c-isotherms, depends on N. Hence, the t_c-isotherms must be different in those two cases. First, attention should be drawn to the unusual form of the t_c-isotherms around $\alpha = 45°$, which manifests itself only at small β. From the physical point of view, it can be explained by a weak change with α of the interplay between CDWs and superconductivity, when those FS areas are affected, where the gap Δ is small, i.e. the near-node regions. From the mathematical point of view, we

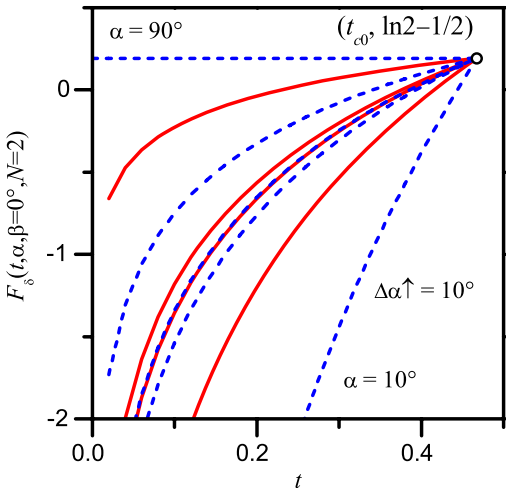

Figure D.2. Crowding of the $F_\delta(t, \alpha, \beta = 0°)$-function profiles at $\alpha = \frac{\pi}{4}$.

should consider formula (B.2) and analyze the combination $z = \alpha + \frac{1}{4}\sin 4\alpha \cos 4\beta$. For a small difference $\zeta = \alpha - \frac{\pi}{4}$, by expanding $\sin 4\alpha$ in a series, we obtain

$$z(\zeta \to 0) \to \frac{\pi}{4} + \zeta(1 - \cos\beta) - \frac{16}{3}\zeta^3 \cos\beta + \ldots. \quad \text{(D.1)}$$

Therefore, if $\cos\beta \approx 1$, which is valid for β in the vicinity of $\beta = 0$, the linear term nearly vanishes and the quantity z becomes almost independent of α. The t-plots of $F_\delta(t, \alpha, \beta \approx 0°, N = 2)$ are concentrated around the dependence $F_\delta(t, \alpha = \frac{\pi}{4}, \beta \approx 0°, N = 2)$, which is depicted in figure D.2. In other words, the profile of the $t_c(\sigma_0)$-dependence turns out to be insensitive to α, the effect being noticeable in figure D.1. As the mismatch angle β grows, the effect becomes less pronounced, which is illustrated in figures D.1(b) and (c).

It is clear that the same phenomenon also arises at $N = 4$. But it is obscured to a great extent by the proximity of the phase plane boundary to the pure CDW state: it forces the isotherms to converge to a point.

References

[1] Vojta M 2009 *Adv. Phys.* **58** 699
[2] Kordyuk A A *et al* 2009 *Phys. Rev.* B **79** 020504
[3] Hoffman J E 2010 *Nature Phys.* **6** 404
[4] Vishik I M, Lee W S, He R-H, Hashimoto M, Hussain Z, Devereaux T P and Shen Z-X 2010 *New J. Phys.* **12** 105008
[5] Kulić M L 2000 *Phys. Rep.* **338** 1
[6] Zhao G-m, Keller H and Conder K 2001 *J. Phys.: Condens. Matter* **13** R569
[7] Bennemann K H and Ketterson J B (ed) 2008 *Superconductivity: Conventional and Unconventional Superconductors* vol 1 (Berlin: Springer)
[8] Bennemann K H and Ketterson J B (ed) 2008 *Superconductivity: Novel Superconductors* vol 2 (Berlin: Springer)
[9] Kordyuk A A, Zabolotnyy V B, Evtushinsky D V, Büchner B and Borisenko S V 2010 *J. Electron. Spectrosc. Relat. Phenom.* **181** 44
[10] Kordyuk A A, Zabolotnyy V B, Evtushinsky D V, Inosov D S, Kim T K, Büchner B and Borisenko S V 2010 *Eur. Phys. J. Spec. Top.* **188** 153
[11] Gabovich A M, Voitenko A I, Ekino T, Suan L M, Szymczak H and Pękała M 2010 *Adv. Condens. Matter Phys.* **2010** 681070
[12] Andrenacci N, Angilella G G N, Beck H and Pucci R 2004 *Phys. Rev.* B **70** 024507
[13] Wulin D, Chien C-C, Morr D K and Levin K 2010 *Phys. Rev.* B **81** 100504
[14] Tinkham M 1996 *Introduction to Superconductivity* (New York: McGraw-Hill)
[15] Mineev V P and Samokhin K V 1999 *Introduction to Unconventional Superconductivity* (Amsterdam: Gordon and Breach)
[16] Schafroth M R, Butler S T and Blatt J M 1957 *Helv. Phys. Acta* **30** 93
[17] Alexandrov A S 2007 *J. Supercond.* **20** 481
[18] Gabovich A M, Moiseev D P and Shpigel A S 1982 *J. Phys. C: Solid State Phys.* **15** L569
[19] Gabovich A M and Shpigel A S 1984 *J. Phys. F: Met. Phys* **14** 3031
[20] Castellani C, Di Castro C and Grilli M 1995 *Phys. Rev. Lett.* **75** 4650
[21] Gabovich A M and Voitenko A I 1997 *Phys. Rev.* B **55** 1081
[22] Gabovich A M, Suan L M, Szymczak H and Voitenko A I 2003 *J. Phys.: Condens. Matter* **15** 2745
[23] Kao Y J, Iyengar A P, Chen Q and Levin K 2001 *Phys. Rev.* B **64** 140505
[24] Manske D 2004 *Theory of Unconventional Superconductors. Cooper-Pairing Mediated by Spin Excitations* (New York: Springer)
[25] Lee P A 2008 *Rep. Prog. Phys.* **71** 012501
[26] Phillips J C 2010 *J. Supercond.* **23** 1267
[27] Gabovich A M, Pashitskii E A and Shpigel A S 1979 *Sov. Phys.—JETP* **50** 583
[28] Gabovich A M and Moiseev D P 1986 *Sov. Phys.—Usp.* **29** 1135
[29] Gabovich A M *et al* 1987 *Fiz. Nizk. Temp.* **13** 844
[30] Gabovich A M and Shpigel A S 1988 *Phys. Rev.* B **38** 297
[31] Machida K 1984 *J. Phys. Soc. Japan* **53** 712
[32] Eremin I and Eremin M 1997 *J. Supercond.* **10** 459
[33] Dahm T, Manske D and Tewordt L 1997 *Phys. Rev.* B **56** 11419
[34] Eremin M V and Larionov I A 1998 *JETP Lett.* **68** 611
[35] Klemm R A 2000 *Physica* C **341–348** 839
[36] Gabovich A M and Voitenko A I 2000 *Low Temp. Phys.* **26** 305
[37] Gabovich A M, Voitenko A I, Annett J F and Ausloos M 2001 *Supercond. Sci. Technol.* **14** R1
[38] Gabovich A M, Voitenko A I and Ausloos M 2002 *Phys. Rep.* **367** 583
[39] Klemm R A 2004 *Nonequilibrium Physics at Short Time Scales: Formation of Correlations* ed K Morawetz (Berlin: Springer) p 381
[40] Tanaka K *et al* 2006 *Science* **314** 1910
[41] Le Tacon M, Sacuto A, Georges A, Kotliar G, Gallais Y, Colson D and Forget A 2006 *Nature Phys.* **2** 537
[42] Boyer M C, Wise W D, Chatterjee K, Yi M, Kondo T, Takeuchi T, Ikuta H and Hudson E W 2007 *Nature Phys.* **3** 802
[43] Koitzsch A *et al* 2010 *Phys. Rev.* B **81** 113110
[44] Gabovich A M and Voitenko A I 2009 *Phys. Rev.* B **80** 224501
[45] Voitenko A I and Gabovich A M 2010 *Fiz. Nizk. Temp.* **36** 1300
[46] Voitenko A I and Gabovich A M 2010 *Fiz. Tverd. Tela* **52** 20
[47] Friend R H and Jérome D 1979 *J. Phys. C: Solid State Phys.* **12** 1441
[48] Vojta M 2010 *Eur. Phys. J. Spec. Top.* **188** 49
[49] Franz M 2004 *Science* **305** 1410
[50] McElroy K, Lee D-H, Hoffman J E, Lang K M, Lee J, Hudson E W, Eisaki H, Uchida S and Davis J C 2005 *Phys. Rev. Lett.* **94** 197005
[51] Robertson J A, Kivelson S A, Fradkin E, Fang A C and Kapitulnik A 2006 *Phys. Rev.* B **74** 134507
[52] Del Maestro A, Rosenow B and Sachdev S 2006 *Phys. Rev.* B **74** 024520
[53] Wróbel P 2006 *Phys. Rev.* B **74** 014507
[54] Zhao H-W, Zha G-Q and Zhou S-P 2008 *New J. Phys.* **10** 043047
[55] Annett J F 1995 *Contemp. Phys.* **36** 423
[56] Damascelli A, Hussain Z and Shen Z-X 2003 *Rev. Mod. Phys.* **75** 473
[57] Markiewicz R S 2005 *Phys. Rev.* B **71** 220504
[58] Tranquada J M, Sternlieb B J, Axe J D, Nakamura Y and Uchida S 1995 *Nature* **375** 561
[59] Zachar O, Kivelson S A and Emery V J 1998 *Phys. Rev.* B **57** 1422
[60] Caprara S, Castellani C, Di Castro C, Grilli M and Perali A 2000 *Physica* B **280** 196
[61] Kohsaka Y *et al* 2007 *Science* **315** 1380
[62] Kivelson S A, Bindloss I P, Fradkin E, Oganesyan V, Tranquada J M, Kapitulnik A and Howald C 2003 *Rev. Mod. Phys.* **75** 1201

[63] Daou R *et al* 2010 *Nature* **463** 519
[64] Krivoglaz M A and Karasevskii A I 1974 *Pis. Zh. Eksp. Teor. Fiz.* **19** 454
[65] Halperin B I and Rice T M 1968 *Solid State Phys.* **21** 115
[66] Hanaguri T, Lupien C, Kohsaka Y, Lee D-H, Azuma M, Takano M, Takagi H and Davis J C 2004 *Nature* **430** 1001
[67] Shen K M *et al* 2005 *Science* **307** 901
[68] Hoffman J E, Hudson E W, Lang K M, Madhavan V, Eisaki H, Uchida S and Davis J C 2002 *Science* **295** 466
[69] Hoffman J E, McElroy K, Lee D-H, Lang K M, Eisaki H, Uchida S and Davis J C 2002 *Science* **297** 1148
[70] Vershinin M, Misra S, Ono S, Ando Y, Abe Y and Yazdani A 2004 *Science* **303** 1995
[71] Fang A, Howald C, Kaneko N, Greven M and Kapitulnik A 2004 *Phys. Rev.* B **70** 214514
[72] Hashimoto A, Momono N, Oda M and Ido M 2006 *Phys. Rev.* B **74** 064508
[73] Ma J-H *et al* 2008 *Phys. Rev. Lett.* **101** 207002
[74] Kato T, Machida T, Kamijo Y, Miyashita R and Sakata H 2009 *J. Phys.: Conf. Ser.* **150** 052101
[75] Wise W D, Boyer M C, Chatterjee K, Kondo T, Takeuchi T, Ikuta H, Wang Y and Hudson E W 2008 *Nature Phys.* **4** 696
[76] Fujita M, Goka H, Yamada K, Tranquada J M and Regnault L P 2004 *Phys. Rev.* B **70** 104517
[77] Fink J *et al* 2009 *Phys. Rev.* B **79** 100502
[78] Li X M, Li F H, Luo H Q, Fang L and Wen H-H 2009 *Supercond. Sci. Technol.* **22** 065003
[79] Sugimoto A, Kashiwaya S, Eisaki H, Yamaguchi H, Oka K, Kashiwaya H, Tsuchiura H and Tanaka Y 2005 *Physica* C **426–431** 390
[80] Bianconi A, Lusignoli M, Saini N L, Bordet P, Kvick Å and Radaelli P G 1996 *Phys. Rev.* B **54** 4310
[81] Castellan J P, Gaulin B D, Dabkowska H A, Nabialek A, Gu G, Liu X and Islam Z 2006 *Phys. Rev.* B **73** 174505
[82] LeBoeuf D *et al* 2011 *Phys. Rev.* B **83** 054506
[83] Vojta M 2011 *Physics* **4** 12
[84] Uchida M *et al* 2011 *Phys. Rev. Lett.* **106** 027001
[85] Borisenko S V *et al* 2008 *Phys. Rev. Lett.* **100** 196402
[86] Inosov D S, Zabolotnyy V B, Evtushinsky D V, Kordyuk A A, Büchner B, Follath R, Berger H and Borisenko S V 2008 *New J. Phys.* **10** 125027
[87] Borisenko S V *et al* 2009 *Phys. Rev. Lett.* **102** 166402
[88] Inosov D S, Evtushinsky D V, Zabolotnyy V B, Kordyuk A A, Büchner B, Follath R, Berger H and Borisenko S V 2009 *Phys. Rev.* B **79** 125112
[89] Brazovskii S A and Matveenko S I 2003 *JETP* **96** 555
[90] Dubroka A *et al* 2011 *Phys. Rev. Lett.* **106** 047006
[91] Gabovich A M and Voitenko A I 2007 *Phys. Rev.* B **75** 064516
[92] Ekino T, Gabovich A M, Suan L M, Pękała M, Szymczak H and Voitenko A I 2007 *Phys. Rev.* B **76** 180503
[93] Ekino T, Gabovich A M and Voitenko A I 2008 *Fiz. Nizk. Temp.* **34** 515
[94] Ekino T, Gabovich A M, Suan L M, Pękała M, Szymczak H and Voitenko A I 2008 *J. Phys.: Condens. Matter* **20** 425218
[95] Brandow B H 2002 *Phys. Rev.* B **65** 054503
[96] Klemm R A 2005 *Phil. Mag.* **85** 801
[97] Zhao G-m 2010 *Phys. Rev.* B **82** 012506
[98] Won H and Maki K 1994 *Phys. Rev.* B **49** 1397
[99] Maki K and Won H 1996 *J. Physique* I **6** 2317
[100] Tsuei C C and Kirtley J R 2008 *Superconductivity: Novel Superconductors* vol 2, ed K H Bennemann and J B Ketterson (Berlin: Springer) p 869
[101] Littlewood P B 1990 *Phys. Rev.* B **42** 10075
[102] Annett J F 1990 *Adv. Phys.* **39** 83
[103] Annett J F 2004 *Superconductivity: Superfluids and Condensates* (Oxford: Oxford University Press)
[104] Leggett A J 2006 *Quantum Liquids: Bose Condensation and Cooper Pairing in Condensed-Matter Systems* (Oxford: Oxford University Press)
[105] Bilbro G and McMillan W L 1976 *Phys. Rev.* B **14** 1887
[106] Ekino T, Gabovich A M and Voitenko A I 2005 *Fiz. Nizk. Temp.* **31** 55
[107] Pickett W E 1989 *Rev. Mod. Phys.* **61** 433
[108] Littlewood P B and Heine V 1981 *J. Phys. C: Solid State Phys.* **14** 2943
[109] Grüner G 1994 *Density Waves in Solids* (Reading, MA: Addison-Wesley)
[110] van Wezel J, Nahai-Williamson P and Saxena S S 2011 *Phys. Rev.* B **83** 024502
[111] Morosan E, Zandbergen H W, Dennis B S, Bos J W G, Onose Y, Klimczuk T, Ramirez A P, Ong N P and Cava R J 2006 *Nature Phys.* **2** 544
[112] Kusmartseva A F, Sipos B, Berger H, Forró L and Tutiš E 2009 *Phys. Rev. Lett.* **103** 236401
[113] Scalapino D J 1995 *Phys. Rep.* **250** 329
[114] Lee W S, Vishik I M, Tanaka K, Lu D H, Sasagawa T, Nagaosa N, Devereaux T P, Hussain Z and Shen Z-X 2007 *Nature* **450** 81
[115] Kondo T, Khasanov R, Takeuchi T, Schmalian J and Kaminski A 2009 *Nature* **457** 296
[116] Kurosawa T *et al* 2010 *Phys. Rev.* B **81** 094519
[117] Hackl A, Vojta M and Sachdev S 2010 *Phys. Rev.* B **81** 045102
[118] Pickett W E, Krakauer H, Cohen R E and Singh D J 1992 *Science* **255** 46
[119] Markiewicz R S, Sahrakorpi S, Lindroos M, Lin H and Bansil A 2005 *Phys. Rev.* B **72** 054519
[120] Abrikosov A A, Gor'kov L P and Dzyaloshinskii I E 1963 *Methods of Quantum Field Theory in Statistical Physics* (Englewood Cliffs, NJ: Prentice-Hall)
[121] Mühlschlegel B 1959 *Z. Phys.* **155** 313
[122] Gabovich A M and Voitenko A I 1995 *Phys. Rev.* B **52** 7437
[123] Yang K and Sondhi S L 1998 *Phys. Rev.* B **57** 8566
[124] Machida K 1981 *J. Phys. Soc. Japan* **50** 2195
[125] Daemen L L and Overhauser A W 1989 *Phys. Rev.* B **39** 6431
[126] Ismer J-P, Eremin I, Rossi E, Morr D K and Blumberg G 2010 *Phys. Rev. Lett.* **105** 037003
[127] Jérome D, Berthier C, Molinié P and Rouxel J 1976 *J. Physique Coll.* **37** C4-125
[128] Levin K, Mills D L and Cunningham S L 1974 *Phys. Rev.* B **10** 3821
[129] Levin K, Cunningham S L and Mills D L 1974 *Phys. Rev.* B **10** 3832
[130] Gabovich A M and Pashitskii E A 1975 *Fiz. Tverd. Tela* **17** 1584
[131] Gabovich A M, Pashitskii E A and Shpigel A S 1976 *Sov. Phys.—Solid State* **18** 1911
[132] Gabovich A M and Voitenko A I 1996 *Physica* C **258** 236
[133] Kondo T, Hamaya Y, Palczewski A D, Takeuchi T, Wen J S, Xu Z J, Gu G, Schmalian J and Kaminski A 2011 *Nature Phys.* **7** 21
[134] Nair S K, Zou X, Chia E E M, Zhu J-X, Panagopoulos C, Ishida S and Uchida S 2010 *Phys. Rev.* B **82** 212503
[135] Ekino T, Sezaki Y and Fujii H 1999 *Phys. Rev.* B **60** 6916
[136] Vedeneev S I, Piot B A and Maude D K 2010 *Phys. Rev.* B **81** 054501
[137] Lubashevsky Y, Garg A, Sassa Y, Shi M and Kanigel A 2011 *Phys. Rev. Lett.* **106** 047002